TU Delft

Delft University of Technology

A Numerical Study on the Significance of Slab for the Response of a Prototype Structure Under Travelling Fires

Nan, Zhuojun; Dai, Xu; Welch, Stephen; Usmani, Asif

DOI
10.1007/s10694-025-01800-3

Publication date
2025

Document Version
Final published version

Published in
Fire Technology

Citation (APA)
Nan, Z., Dai, X., Welch, S., & Usmani, A. (2025). A Numerical Study on the Significance of Slab for the Response of a Prototype Structure Under Travelling Fires. *Fire Technology*, *61*(7), 5557-5588. https://doi.org/10.1007/s10694-025-01800-3

Important note
To cite this publication, please use the final published version (if applicable).
Please check the document version above.

Copyright
Other than for strictly personal use, it is not permitted to download, forward or distribute the text or part of it, without the consent of the author(s) and/or copyright holder(s), unless the work is under an open content license such as Creative Commons.

Takedown policy
Please contact us and provide details if you believe this document breaches copyrights.
We will remove access to the work immediately and investigate your claim.

This work is downloaded from Delft University of Technology.
For technical reasons the number of authors shown on this cover page is limited to a maximum of 10.

Fire Technology
https://doi.org/10.1007/s10694-025-01800-3

A Numerical Study on the Significance of Slab for the Response of a Prototype Structure Under Travelling Fires

Zhuojun Nan[1] · Xu Dai[2] · Stephen Welch[3] · Asif Usmani[4]

Received: 28 May 2024 / Accepted: 19 August 2025
© The Author(s) 2025

Abstract
"Travelling fires" discriminate a fire plume at the near-field and a hot smoke layer pre-heating the ceiling at the far-field, with the intent of ensuring the robustness of structural design for large compartments under realistic fires. Once the fire is "travelling", the near-field has a leading edge representing the fire spread, and a trailing edge representing the burnout of the fuel. Despite the recognised effects of travelling fires, the mainstream of efforts into their effect on structural response has been limited to 2D models using the finite element method (FEM). This paper aims to identify the importance of slab inclusion with a 3D FEM structural model for steel-composite structures under travelling fires, assessed against the corresponding simplified 2D structural frame models (i.e., with and without effective slab in the 2D steel frame model). The first step is a comparative structural analysis of a prototype composite structure under various design fire scenarios, including standard fire, parametric fires and travelling fires. The role of the fire protection scheme for the simplified 2D models against the 3D model for the numerical predictions is also explored. It is found that the structural load path, and the potential structural failure mechanisms, could be fundamentally different between the 3D model and the simplified 2D models. Although the 2D frame model tends to predict larger deflections (i.e., more conservative) than the 3D model, it could also significantly underestimate the large internal forces from the beams, so that the connections' failure under travelling fires might be overlooked. Further, due to the simplification of the 2D models in omitting the significant stiffness contribution from the slab and the adjacent structural components, the effect of the fire protection is likely to be amplified. This may give misleading information on the performance-based structural fire design under different travelling fire scenarios. Hence, the 3D model can be considered as feasible but also necessary for structural fire analysis for travelling fires as a complement to the simplified 2D model approach.

Keywords Travelling fires · 3D FEM · Steel-composite structure · Performance-based design

Extended author information available on the last page of the article

Published online: 16 September 2025

1 Introduction

In structural fire engineering, the "travelling fire" methodology has been gradually accepted as an appropriate fire boundary condition for structural member calculations for large open-plan compartments [1]. Over the past three decades, various theoretical models of travelling fires have been formulated in response to fire incidents and experimental studies. A pioneer, the Clifton's travelling fire model, proposed in 1996, consists of a sequence of parametric fires with time lags [2]. However, the applicability of this simplified model is limited. Subsequently, Rein et al. developed a more explicit representation of the two fire regimes, with a series of enhancements: the Travelling Fires Methodology (TFM) [3, 4], its improved version (iTFM) [5] and the version with flame extension (fTFM) [6]. In the TFM and its subsequent refined versions, the near-field represents the flames directly impinging on the ceiling and assumes the peak flame temperatures as 800–1200 °C. Alpert's ceiling jet correlations [7] are adopted for calculating the far-field smoke temperature. Although the TFM reflects the non-uniform temperature distribution and the long fire durations observed in real fire incidents, it also has limitations, such as not accounting for the impact of discontinuous fuel load distributions and different ventilation conditions on the resultant heat release rate [8]. In 2016, Dai et al. [9] established the Extended Travelling Fire Methodology (ETFM) framework. The ETFM integrates a "mobilised" version of Hasemi's localised fire model [10] for near-field plume analysis, and a simplified smoke layer calculation using the FIRM zone model [11] for the far-field. Considering both energy and mass conservation, the efficacy of the ETFM framework in simulating the thermal response of structural elements under travelling fire conditions was benchmarked [9] against results from the Veselí Travelling Fire Test [12]. Additionally, Charlier et al. introduced an analytical model combining the concept of a virtual solid flame (with different fire development stages) with a zone model (representing hot gases at upper levels) [13], capturing some of the TRAFIR test nº2 [14] experimental results. Recent developments, such as GoZone [15] and a natural fire model in OpenSees for fire [16], offer enhanced descriptions of fire phases in large open-plan compartments, ranging from ignition to various stages of growing, "travelling" and intense burning. Computational Fluid Dynamics (CFD) simulations have also contributed to understanding complex fire dynamics in such environments [12, 17], leading to a more detailed characterisation of fire spread validated against large-scale travelling fire tests. Nonetheless, the evolution of modern architecture continues to influence the fire dynamics expected in large open-plan compartments, challenging conventional modelling assumptions. For instance, the increasing use of sustainable construction materials, such as timber, in structural elements introduces a fundamental shift in the dynamics of compartment fires, as evidenced by the outcomes of the CodeRed fire tests [18].

Considering the demand for effective numerical simulations which can be undertaken within the constraints of limited computational resources and time, 2D models using beam elements are a potentially attractive approach. They can also show good qualitative agreement with 3D models and, in some cases, provide conservative predictions for deflections by neglecting the composite action between the beams and the concrete floor slab [19]. This makes 2D models useful for early-stage structural fire analysis in complex structures, such as high-rise buildings, where developing a full 3D model would be computationally expensive and time-consuming. However, an over-simplified structural model cannot compensate for a more representative fire scenario, as is the prevailing situation for travelling fires for

performance-based structural engineering. For instance, Rezvani & Ronagh [20] and Rackauskaite et al. [8, 19, 21] performed extensive numerical studies on structural response of steel-framed buildings, using 2D generic frame structures under the TFM [3, 4] and the iTFM [5]. These studies are practically limited in applying travelling fires on 2D structural models, which cannot represent the complexity of behaviours presented in a realistic structure, such as the membrane behaviour of floor systems.

More importantly, the Cardington fire tests clearly showed that the slabs carried most of the load at very high temperatures [22]. Jiang and Li [23, 24] compared the progressive collapse analysis of steel frames with concrete slabs exposed to a localised fire between 2D and 3D models. The results demonstrated that the collapse modes and load redistribution path of the 2D model and 3D model were fundamentally different. Jiang et al. [25] further investigated the disproportionate collapse of a 3D steel-framed gravity building under three travelling fire scenarios (using Clifton's travelling fire model [2]). It was found that a higher level of fire protection may prevent the collapse of structures but may also lead to structural failure in the cooling phase due to the delayed increment of temperatures in the heated members. A lack of understanding persists about the effect of fire protection on failure mechanisms between 2D and 3D FEM models under various travelling fire scenarios.

This paper aims to identify the importance of concrete slab inclusion by using a 3D FEM structural model for steel-composite structures under travelling fires, with a special emphasis on the significance of ignoring the slab structural capacity contribution for the corresponding simplified 2D structural frame models. Further, the paper investigates such structural behaviour differences under various design fire scenarios, i.e., standard fire, parametric fires and travelling fires. This study further addresses the role of the fire protection scheme on numerical predictions of thermal and structural responses for performance-based structural fire design.

2 Methodology

2.1 The Structural Model

Inspired by the BST/FRS 1993 travelling fire test structural layout [26], a prototype structure representing a "slice" of a steel framed building with composite floors was developed, see Fig. 1a. It has structural dimensions of 23.00 m length × 6.00 m width × 2.75 m height, with three bays. This structure was designed by following the Eurocode to resist ambient design load on the floor (1.35×4.13 (dead load) $+ 1.50 \times 2.50$ (live load) $= 9.30$ kN/m^2). The cross-section of all floor beams and columns were chosen as UB $406 \times 178 \times 54$ with steel grade S355. The Cofraplus 60 [27] composite slab with thickness of 140 mm is used.

This study employs an LS-DYNA 3D modelling approach [28], validated against the global behaviour measured at mid-span deflections from the Veselí Travelling Fire Test and previous Vulcan modelling results by Horová and Wald [29]. Further validation details (while the structure is under the fire limit state) can be found in reference [28]. In this study, the LS-DYNA 3D model simplifies the composite slab as the equivalent self-weight of flat concrete slab with a continuous depth of 110 mm concrete C30/37, reinforced by two structural mesh fabric B503 (i.e., 503 mm^2/1000 mm) placed 25 mm from the edges of the cross-section. The design of reinforcement B503, with a reinforcement ratio of approxi-

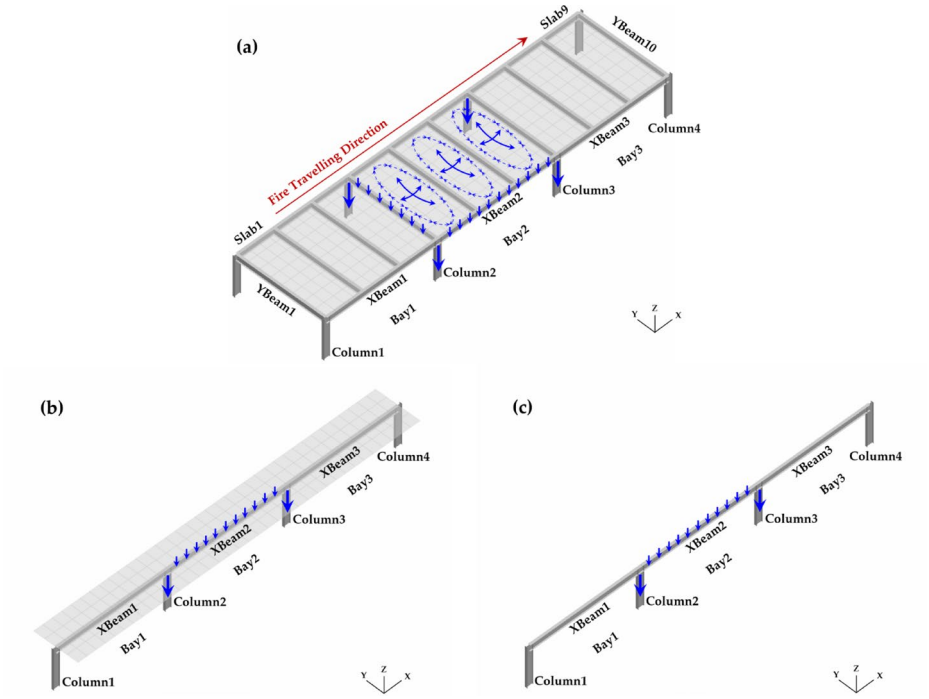

Fig. 1 Schematic of the prototype structure load path in the second bay: **a** 3D model; **b** 2D model with effective slab width; and **c** 2D steel frame model

mately 0.005 in the longitudinal direction, falls within the typical reinforcement ratio range of approximately 0.004 to 0.008 [30]. The relatively large reinforcement in both the upper and lower layers of the slab cross-section not only supports the use of thin slabs with high reinforcement ratios, allowing for large deflections, but is also beneficial for managing the complex stress redistribution that occurs during a fire. As the fire spreads, the regions of compression and tension in the slab shift significantly due to heating and cooling, necessitating such a reinforcement design. The beam elements share the same nodes with the shell elements to account for composite action effects. The formulation of steel structural members and slabs were Hughes-Liu and Belytschko-Lin-Tsay, respectively. In the LS-DYNA model, the materials of steel and concrete were modelled using MAT_202: Steel_EC3 and MAT_172: CONCRETE_EC2, with thermal properties (e.g., thermal conductivity, specific heat capacity, thermal expansion, Young's modulus, and the stress-strain relationship at elevated temperatures) defined according to the Eurocodes [31, 32]. Type 7 siliceous aggregate was used for the stress-strain-temperature relationship for concrete, as per EN 1992-1-2:2004, for fire engineering analysis. In LS-DYNA R9, the maximum allowable cracks are set at 2. In our model, the strain required to fully open a crack was defined as 0.0025, which falls within the typical range observed for concrete exposed to elevated temperatures. The model accounts for concrete damage at elevated temperatures, including the consideration of cracking [33]. It should be noted that LS-DYNA automatically adjusts parameter values based on temperature. During the cooling phase, these parameters (i.e., material properties) of steel revert to their values at lower temperatures (but plastic strains are still kept), without

accounting for the material's degradation and changes after exposure to heat. This represents a limitation in the current numerical model, as it does not fully capture the complexities of material behaviour during the heating-cooling cycle in a fire. Further development of material models that incorporate the cooling effect should be considered for establishing more robust and comprehensive modelling approaches in future work. All the connections were modelled as pinned.

Notably, the effects of continuity and restraint from adjacent structures on the extracted "slice" of the steel frame building with composite floors were not represented in the numerical models. This may contribute to a potentially early structural failure under fire due to the absence of the horizontal constraints that would typically be present. The mechanical boundary conditions are complex, particularly when simplifying structural models in various ways, including the 3D model and 2D models with or without slabs. Therefore, this study focuses on comparing the performance of 3D versus 2D models, intentionally excluding the differences caused by the boundary condition simplifications themselves.

The complexity of structural-fire responses may require the use of simplified 2D models, as opposed to the more detailed 3D models, for effective analysis and design. Previous studies [8, 19–21, 24, 25] have employed two methods to simplify 3D structural models into 2D models, i.e., (1) using an effective width approach to represent the behaviour of the composite slab in accordance with the Eurocode [34], and (2) using a simplified steel frame model that neglects the contribution of the slab to the overall structural capacity.

The corresponding simplified 2D models with three spans (7.5 m, 8.0 m and 7.5 m) were extracted from the longitudinal direction of the 3D prototype structure, i.e., XBeams with the longest beam span in the 3D model and columns, as shown in Fig. 1b and c. Besides, similarly as [19], the heat sink effect due to the concrete slab was considered in the heat transfer analysis of the simplified 2D models. As shown in Fig. 1b, in the 2D model with effective slab width, the reinforced concrete slab with a width of 2.0 m (i.e., span/4 of the longest primary beam [35]), was modelled to represent the composite beam. In the 2D steel frame model, as shown in Fig. 1c, the concrete slab and the composite action between the beams and the slab were not considered. Nevertheless, the load from the concrete slab was still considered in the 2D models, which could have resulted in an equivalent mechanical load compared to the 3D model. A mesh sensitivity analysis was conducted to ensure both modelling accuracy and time efficiency. For the 3D model, each slab shell element was divided into 32 meshes, 4 in the length direction (X direction) and 8 in width direction (Y direction), as shown in Fig. 1. Beam elements were meshed to match the corresponding shell element lengths, and each column was divided into 4 meshes. The same meshing approach was applied to the 2D models. The duration of travelling fire was scaled by a time factor of 1/1000 for the explicit dynamic analysis following the "lessons learnt" in LS-DYNA by Rackauskaite et al. [36]. To avoid inertia effects from thermal expansion and large deflections caused by rapid temperature increases, a linear ramping of the load over time was applied to reduce numerical instabilities and approach a quasi-static solution. Additionally, damping was applied in the structural model to dissipate kinetic energy, allowing the use of scaled thermal load durations [36]. Given the expectation that the thermomechanical response would be pseudo-static throughout most of the fire, dynamic events were considered secondary in this model [37].

Fire protection is a design parameter having a significant effect on the structural behaviour under travelling fires. For conventional fire resistance design, the general approach is

to protect all structural steel members to achieve a prespecified fire resistance rating (FRR) according to the building use and height. However, instead of protecting all steel members, only the columns and primary beams were protected in this study while leaving the secondary beams unprotected. This fire protection scheme is to encourage the development of the tensile membrane action [38–41], which has increasingly been considered in practical projects for performance-based structural fire design of steel-composite floor systems. The effect of such a fire protection scheme on the structural response for both the 3D and 2D models under travelling fires is also investigated in detail in Sect. 5. In this study, the thickness of the fire protection was required to deliver an equivalent FRR for structural components. The fire protection thickness is based on the simplified calculation in Eurocode 3 [32]. The sprayed mineral fibre of 15 mm thickness is adopted, with thermal conductivity 0.12 W/(m·K), density 300 kg/m^3 and specific heat 1200 J/(kg·K) following the recommendations from Franssen et al. in 2009 [42]. Note that all primary beams and columns are protected to achieve at least a one-hour FRR (i.e., R60).

2.2 The Design Fire Scenarios

Various types of design fires are considered in this study, including the ISO 834 standard fire curve and the Eurocode parametric fires [43]. Moreover, travelling fire scenarios are also addressed using the Extended Travelling Fire Methodology (ETFM) framework, which considers both the energy balance and mass balance of the large compartment compared with other travelling fire models [1, 9]. In OpenSees, gas temperatures generated from the fire models are converted to heat fluxes, accounting for both convection and radiation, and applied as thermal boundary conditions for the heat transfer analysis. In this study, the convective heat transfer coefficient and surface emissivity were set to 25 W/(m^2·K) and 0.7, respectively. The thermal conductivities of the steel and concrete materials at elevated temperatures followed the Eurocode. The exposed surfaces of the composite slab are depicted in Fig. 2a. For heat transfer analysis in OpenSees, 15 data points from a 2D I-beam and 9 data points from a 1D slab were used to extract time-temperature data, as shown in Fig. 2b, c. Additionally, the cross-sectional heat transfer analysis of I-beams and slabs was validated against experimental measurements from full-scale composite floor systems exposed to fires in large enclosures, as conducted by the National Institute of Standards and Technology (NIST) at the National Fire Research Laboratory [44].

2.2.1 Standard Fire and Parametric Fires

Figure 3 summarises the time-temperature curves in this study with a uniform temperature distribution in the compartment, i.e., standard fire and parametric fires [43]. Note that the

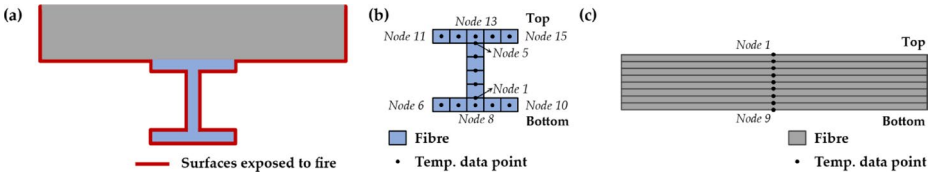

Fig. 2 Schematic for heat transfer analysis in OpenSees: **a** Fire-exposed surfaces; **b** Temperature data points and fibres in the I-beam; and **c** Temperature data points and fibres in the slab

duration of the standard fire is limited to 60 min, corresponding to the assumed fire resistance of the beams in this study.

The parametric fires are determined according to the compartment conditions of the BST/FRS 1993 travelling fire test [26], i.e., a fire load density for offices, i.e., 511 MJ/m^2. The intensity and duration of the design parametric fire scenarios are varied by changing the opening factor ($O=A_wH^{1/2}/A_t$ ($m^{1/2}$)) (i.e., opening sizes, assuming a window height of 1.0 m). Two Eurocode parametric curves, namely "Short-hot" and "Long-cool" fires, are considered [45]. The Short-hot fire, with an opening factor of 0.08 $m^{1/2}$, exhibits high temperatures (maximum temperature of 1284 °C) but a relatively short duration of approximately 37 min. In contrast, the Long-cool fire, with an opening factor of 0.02 $m^{1/2}$, provides less ventilation, resulting in a lower maximum temperature of 1091 °C but a longer duration of around 252 min. To ensure the "consistency" between the assumed parametric fires and the travelling fires, a parametric fire curve with opening factor of 0.06 $m^{1/2}$ is used to approximate the "Short-hot", as this opening factor is equivalent to an inverse opening factor ($IOF=A_wH^{1/2}/(A_t - A_v - A_{floor})$ ($m^{-1/2}$))=9.6 which is the opening condition which was assumed for the design travelling fires in this study. Note that the parametric fire curve with opening factor of 0.06 $m^{1/2}$ is still a close representation of Short-hot defined in reference [45], see Fig. 3.

2.2.2 Travelling Fire

A more advanced travelling fire model, the Extended Travelling Fire Methodology (ETFM) framework [9] was applied in this study. Both the travelling fire modelling and subsequent heat transfer analysis were carried out using OpenSees [9]. The fire was assumed to start at the left short end of the compartment, travelling along the longitudinal direction (i.e., left to right as shown in Fig. 4).

To investigate the structural response under travelling fires, representative scenarios were defined first. For this study, it is critical that the selected fire scenarios are likely to

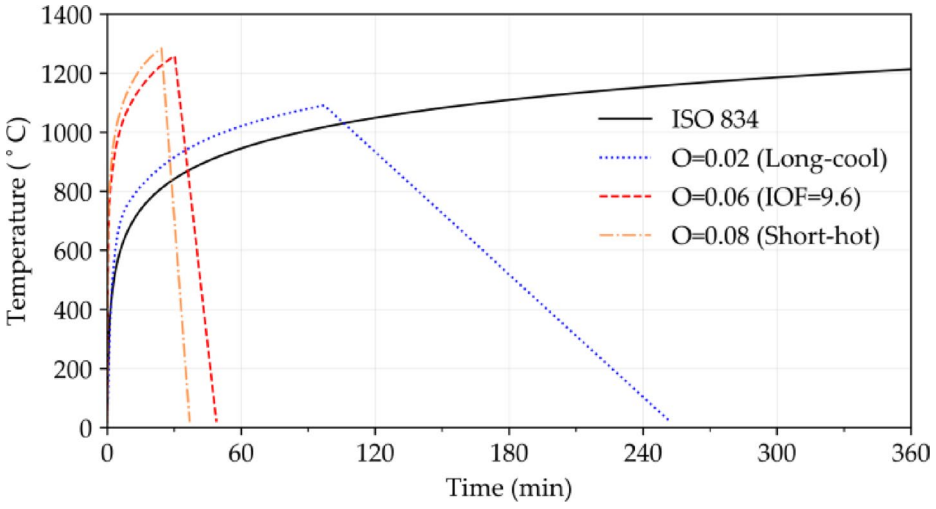

Fig. 3 Time-temperature curves: ISO 834 standard fire, and the parametric fires (Short-hot, Long-cool, IOF=9.6)

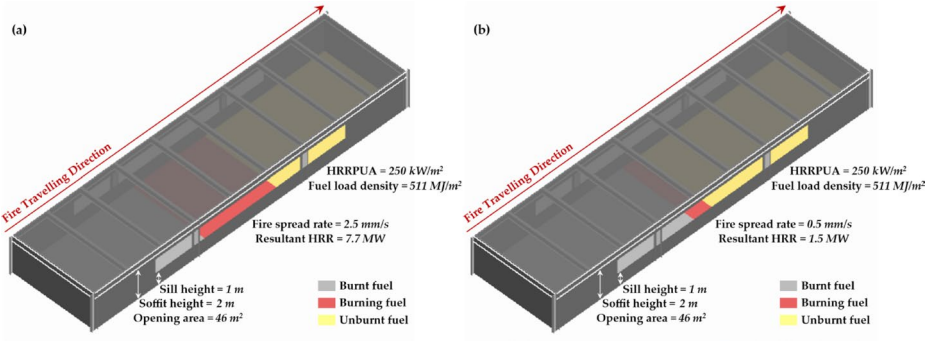

Fig. 4 The demonstration of travelling fire scenarios: **a** Travelling fire scenario 1 (2.5 mm/s); and **b** Travelling fire scenario 2 (0.5 mm/s)

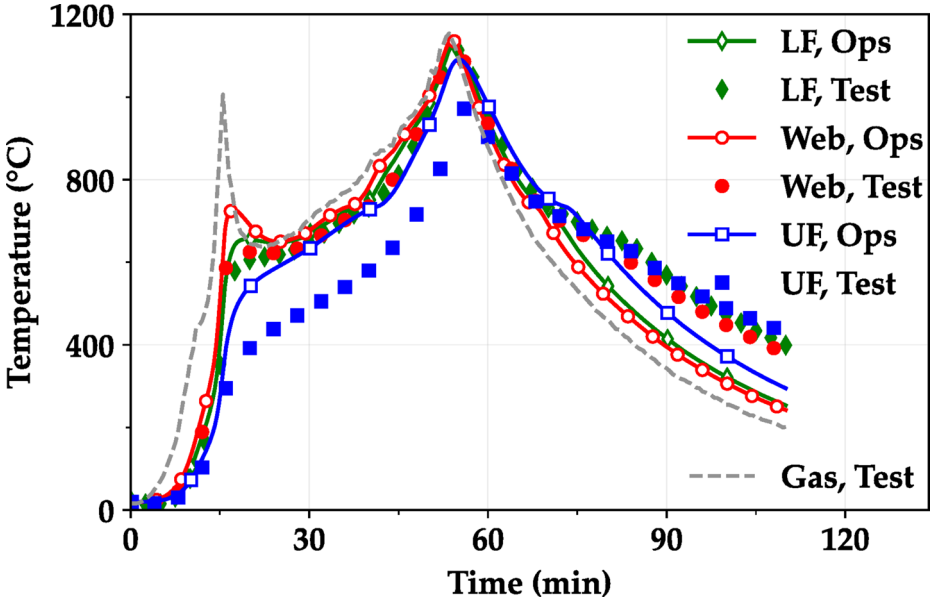

Fig. 5 Comparison of heat transfer analysis results using OpenSees [16] with experimental data of an unprotected beam at Crib 2 from the BST/FRS 1993 travelling fire test 2 [26]. (*Note: LF* = Lower flange; *UF* = Upper flange; *Ops* = OpenSees)

challenge the prototype structure to its failure. The relevant parameters of travelling fire scenarios were selected for typical office buildings [43, 46, 47]: fuel load density 511 MJ/m^2, heat release rate per unit area (HRRPUA) 250 kW/m^2, inverse opening factor (IOF) 9.6, total heat loss fraction 0.85 and radiative heat loss fraction 0.35. Travelling fire spread rates are among the most important parameters for the structural fire design, due to their potentially high influence on the thermal and the structural response [9, 28]. Hence, this paper investigates different fire spread rates and the corresponding structural performance for the 2D and 3D models. Within the typical range of fire spread rates, i.e., between 0.1 and

19.3 mm/s based on the previous experimental results [5], two representative travelling fire scenarios, as shown in Fig. 4, were selected for the ETFM framework:

1. Scenario 1: fire spread rate 2.5 mm/s (with resultant HRR 7.7 MW).
2. Scenario 2: fire spread rate 0.5 mm/s (with resultant HRR 1.5 MW).

2.3 Summary of Numerical Investigation Cases

This study first focuses on comparing the structural fire responses of models without fire protection layers, in Sects. 3 and 4. In Sect. 3, this comparison is crucial for understanding how the 3D structural model responds to both "uniform" design fires and more realistic travelling fires. Section 4 further explores the importance of slabs in influencing structural responses, specifically by comparing the 3D model to 2D models under travelling fire scenarios. Moreover, it lays the groundwork for evaluating the effectiveness of fire protection design in different structural models (3D vs. 2D) under travelling fires, as discussed in Sect. 5.

It should be noted that this study adopts multiple failure criteria to analyse structural responses under various design fire scenarios, providing a more comprehensive assessment of fire-induced structural failure. This approach aligns with previous research [19, 48], which similarly utilises multiple criteria to investigate structural performance under fire. Meanwhile, our previous study [28] suggests that relying on a single criterion is insufficient to ensure adequate structural fire design, particularly for travelling fires. The multiple failure criteria include critical temperature, critical deflection, critical deflection rate and stress utilisation. While these criteria are applied at the element level, they collectively enhance the understanding of global structural behaviour under fire, including the potential for progressive collapse. The critical temperature of 550 °C is assumed for composite beams supporting concrete floor slabs when the building occupancy is not specified [49]. The critical temperature of 160 °C for unexposed concrete slab surfaces is defined based on the ASTM E119 [50]. The critical deflection is calculated as L/20, and the critical deflection rate is calculated as L2/9000d, where L is the length of the beam. The stress utilisation at the mid-span of the beam is defined as one of the failure criteria of a single element [28], i.e., the ratio of the axial stress envelope in the whole beam cross-section over the steel yield strength. The failure is defined as the beam reaches its yield capacity at ambient temperature (i.e., 355 MPa at 20 °C) and can no longer support the structure above [51], i.e., the stress utilisation reaches 1.0. These criteria are applied to individual structural components, including both steel beams and concrete slabs. By employing these criteria, it becomes possible to more comprehensively assess the failure of key structural elements, which, in turn, enables the prediction of global structural responses and the potential for progressive collapse.

3 Structural-fire Behaviours Under Design Fire Scenarios

This section builds upon the preceding section in exploring the behaviour of the steel-composite prototype structure without fire protection when exposed to various design fires, as outlined in Sect. 2, including a range of fire boundary conditions, i.e., the ISO 834 standard fire, parametric fires and travelling fires (using the ETFM framework). Despite steel's non-

combustible nature, its performance under fire conditions, especially without fireproofing, often falls short of requirements. When exposed to rapidly increasing temperatures, steel structures are vulnerable to failure, particularly under "uniform" design fires where the temperature of all structural elements rises quickly, potentially triggering the progressive collapse of the entire structure. These critical issues will be the focus of Sects. 3 and 4. Kindly note that in real-life design, a certain level of fire protection is still needed. This research deliberately omitted the fire protection to enhance the comparison studies on 2D simplified frame models against the 3D models with inclusion of steel-concrete composite floor structure. Fire test results [14, 26] indicate that the heating and cooling rates of steel structural members under travelling fires are not significantly slower than the surrounding gas temperature changes, albeit with a small offset in time. The temperature increase in unprotected steel members closely follows the measured gas temperature, with a slight delay and a lower peak due to heat transfer. During the cooling phase, the temperature decrease in steel members is slower than that of the surrounding gas, as shown in Fig. 6. However, the overall trend remains consistent.

Furthermore, the heat transfer analysis has been validated using OpenSees [16] against experimental data from the BST/FRS 1993 travelling fire test 2 [26]. Figure 6 demonstrates that the model effectively captures the heating of steel beams. While the heat transfer analysis predicts a faster cooling rate for steel beams compared to experimental results, the overall trend and error margin remain reasonable. The model reliably represents the thermal response of unprotected steel structural members under travelling fires.

3.1 "Uniform" Design Fires

3.1.1 Standard Fire (ISO 834)

Under the ISO 834 standard fire exposure, assuming a spatially uniform distribution of gas-phase temperature, the thermal responses of structural members are identical (when the cross-sections and materials are the same). Figures 6a and c show the temperature development across the cross section of the I-beam and slab, respectively, under ISO 834 standard fire.

The displacement development of the 3D model subjected to the standard fire (ISO 834) is presented in Fig. 7. As expected, the displacement of the structure increases with rising temperature due to the weakening and softening of the steel members. As observed in Fig. 7,

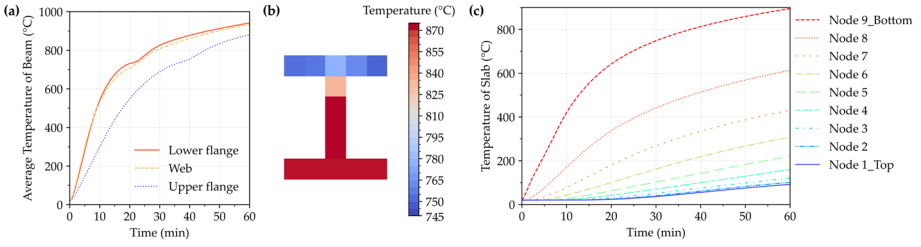

Fig. 6 Thermal response of the structural elements in 3D model under the standard fire (ISO 834): **a** Average temperature of the I-beam lower flange, web and upper flange; **b** Temperature distribution across the I-beam cross section at 40 min; and **c** Temperature development in the slab cross section

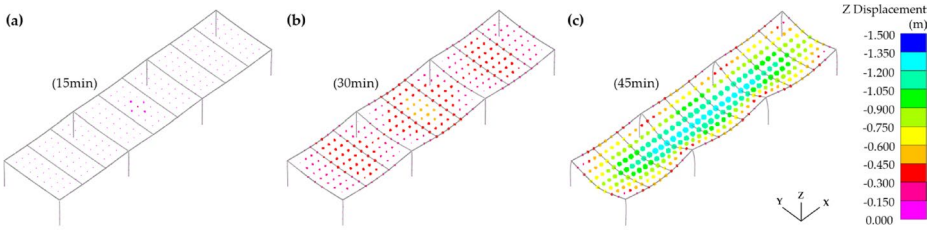

Fig. 7 Displacement contour under the standard fire (ISO 834)

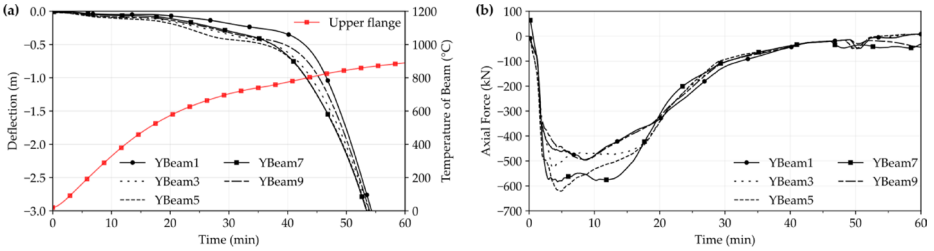

Fig. 8 Structural response of the YBeams (Y direction) in 3D model at mid-span under the standard fire (ISO 834): **a** Deflection; and **b** Axial force

the deflections in the middle bay are slightly larger compared to the neighbouring bays. This discrepancy is attributed to the relatively longer span of 8.0 m in Bay 2, in contrast to the 7.5 m spans in Bay 1 and Bay 3. Consequently, YBeam5 and YBeam7 in Bay2 fail earlier, characterised by rapidly increasing deflections, see Fig. 8a. Specifically, the deflection rate of YBeam5 continuously escalates, beginning at 8.1 mm/min after 31 min of standard fire exposure. Similarly, the deflection rate of YBeam7 increases from 18.4 mm/min starting at 32 min of exposure.

Figure 8a demonstrates that the deflection of the YBeams (referring to the beams in the latitudinal direction of the compartment, as shown in Fig. 1) increase with the elevation of the beam temperature. Once the upper flange temperatures of the beams are close to 800 °C, the deflection of the YBeams increase rapidly as "run-away" at around the 40 min, indicating the occurrence of progressive collapse. At this stage, the temperature across the entire beam section ranges from 750 °C to 880 °C (see Fig. 8b), causing the steel material to lose over 90% of its strength [32], rendering the steel beams incapable of bearing loads. Figure 8b demonstrates that, as the temperature rises, the YBeams experience compression with increased axial forces up to 600 kN. However, after 15 min of exposure, the axial force of the YBeams decreases due to significant strength reduction at elevated temperatures, resulting in a loss of bending strength. Consequently, with the continuous development of deflections, the compressive force rapidly decreases, eventually transitioning to tension as the beams primarily support loads through catenary action.

3.1.2 Parametric Fires (Long-cool and "Short-hot (with IOF 9.6)")

Parametric fires, despite accounting for some fire dynamics and compartment conditions (e.g., opening size and thermal inertia of the compartment linings), were originally devel-

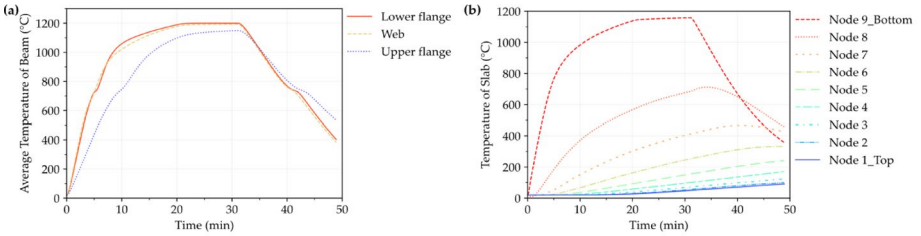

Fig. 9 Thermal response of the structural elements in 3D model under Short-hot (with IOF 9.6): **a** Average temperature of the I-beam lower flange, web and upper flange; and **b** Temperature development in the slab cross section

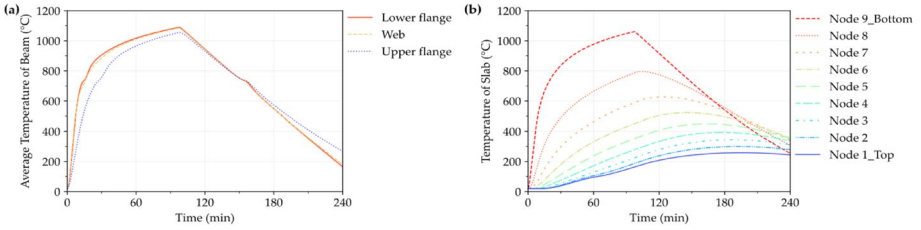

Fig. 10 Thermal response of the structural elements in 3D model under Long-cool: **a** Average temperature of the I-beam lower flange, web and upper flange; and **b** Temperature development in the slab cross section

oped based on scaled compartment fire tests that assume a uniform temperature distribution. Hence, it is more suitable for post-flashover fires in compartments with sizes up to 500 m^2 [9]. Figures 9 and 10 demonstrate the thermal responses of the steel beams and slabs under the Short-hot (with IOF 9.6) and Long-cool parametric fires, respectively. It is important to note that the definition of thermal properties according to Eurocode 3 [32], as mentioned above does not extend to steel temperatures above 1200 °C. Consequently, in the OpenSees heat transfer analysis, the steel temperature is capped at a maximum of 1200 °C. This adjustment explains the plateau observed in the average temperature of the beam's lower flange and web under the Short-hot (with IOF 9.6) parametric fire, as shown in Fig. 9a.

Figures 11 and 12 illustrate the structural response of the YBeams under two different parametric fire scenarios, the Short-hot (with IOF 9.6) and Long-cool, respectively. Despite variation in input parameters, the structural response under these two parametric fire scenarios, including deflection and axial force of the structural beams, is quite similar. This similarity arises from the fact that the parametric fires still provide uniform gas-phase temperatures. Furthermore, as the structure is left unprotected, both parametric fire scenarios result in structural failure during the heating phase, when the upper flange temperature approaches 800 °C. At this point, the maximum temperature at the bottom flange often surpasses 1000 °C. This increase in temperature causes steel to lose more than 90% of its proof strength [32], leading to beam failure, as indicated by rapidly increasing and "runaway" deflections, demonstrated in Figs. 11a and 11a. The failure times for the Long-cool and Short-hot (with IOF 9.6) are at approximately 10 min and 30 min respectively, due to

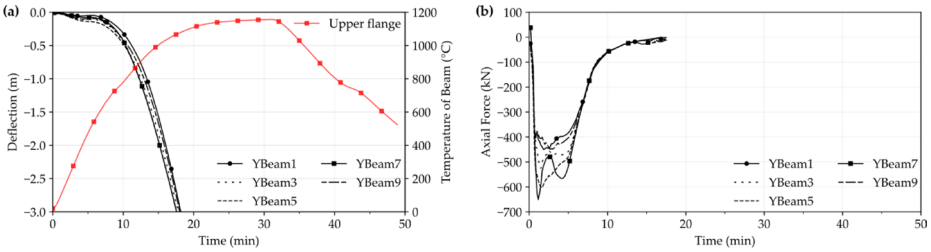

Fig. 11 Structural response of the YBeams (Y direction) in 3D model at mid-span under Short-hot (with IOF 9.6): **a** Deflection; and **b** Axial force

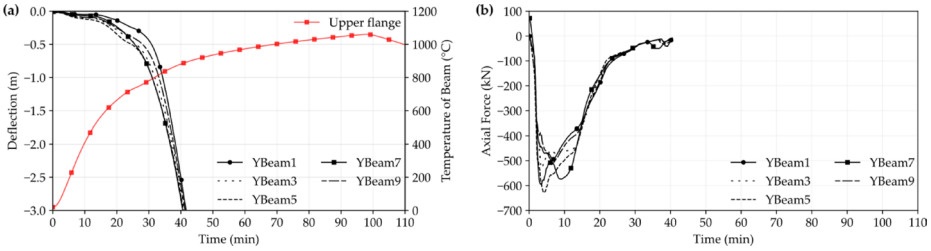

Fig. 12 Structural response of the YBeams (Y direction) in 3D model at mid-span under Long-cool: **a** Deflection; and **b** Axial force

the distinct gas-phase temperature development of the parametric time-temperature curves under different opening conditions, as discussed in Sect. 3.1.

These findings highlight that, although various design fire scenarios with uniform heating were considered, there is no significant impact on the structural fire behaviour in these cases. This suggests that uniform design fire scenarios might only represent a limited range of more complex fires and may not be sufficiently representative for structural fire design in practice.

3.2 Travelling Fires

3.2.1 Travelling Fire Scenario 1 (2.5 mm/s)

Travelling fire scenario 1 represents a design fire scenario with a resultant HRR of 7.7 MW, which is higher than the typical design value of 5.0 MW for commercial buildings [52]. Here, the fire duration for each bay is around 60 min with a fire spread rate of 2.5 mm/s. It could provide sufficient heating and cooling time for the structural members, and satisfy the general requirements of structural fire design for fire resistance rating (FRR) (i.e., R60) [34].

Figure 13 summarises the time-temperature histories of the beams and slabs along the travelling fire path in the 3D model, specifically focusing on the lower flange of beams and the bottom surface of slabs. Full heating and cooling cycles are induced by the travelling fire on the structure. In Fig. 13a, the beams in the latitudinal direction of the compartment (i.e., Y direction refers to Fig. 1) have a peak temperature of 820 °C, exceeding the critical temperature of 550 °C. YBeam1 and YBeam10 have relatively lower peak temperatures,

i.e., approximately 665 °C, as these beams are at the edge of the compartment during the travelling fire initial developing and decaying stages. In Fig. 13b, note that none of the slab top surfaces reaches its critical temperature, i.e., 160 °C. It should be mentioned that the temperature of the steel beams connected to the columns is multiplied by a reduction ratio of 0.7 to estimate the column temperature, assuming a uniform temperature distribution across the column. The rationale for applying the 0.7 reduction factor is that columns typically require larger cross-sections or thicker fire protection layers to enhance fire resistance; however, in our design structures, the column and beam cross-sections are identical. Given the complexity of conducting 3D heat transfer analyses on columns, particularly under travelling fires, this simplification aligns with our earlier work [28, 29].

Figure 14 presents the displacement development of the 3D model under the travelling fire scenario 1. For this figure, critical structural response events at specific times are selected and demonstrated: 35 min, 95 min, 155 min, and 245 min. Note that scenario 1 has entered the cooling phase at 245 min. In general, the deflection sequence of the steel beams follows the travelling fire trajectory, i.e., as the fire travelled to each beam it would have the largest deflection; as the fire travels away from each beam, the deflection would decrease due to cooling. As shown in Fig. 15a, YBeam1 has the lowest deflection of 0.08 m at 38 min, in contrast YBeam5 has the largest deflection of 0.28 m at 241 min. It should be noted that the second bay which has a slightly longer span (i.e., 8.0 m) has the largest deflection compared to the other two neighbouring bays with 7.5 m span. This is because the longer primary beams of the second bay have larger deflections in the heating phase due to the thermal expansion. The thermal expansion of the longer primary beams is restrained by the neighbouring cooler bays; hence, a relatively larger residual deflection of 0.33 m is also induced at the second bay in the cooling phase.

As revealed in Fig. 15b, all beams experience "axial force reversal" sequentially. Namely, the beams are subjected to compressive force during the heating phase and tensile force during the cooling phase, triggered by the movement of the travelling fire near-field beneath the steel beams. YBeam7, for example, experiences large axial forces, such as 650 kN (in compression) and 2311 kN (in tension) at 25 min and 200 min, respectively.

The membrane tractions in the slab of the 3D model at selected times under travelling fire scenario 1 are presented in Fig. 16. The red shaded area represents the fire size, i.e., approximately 30 m^2. In Fig. 16a–c, the 3D model is subjected to travelling fire direct flame for the near-field, and pre-heated by the smoke layer for the far-field. The composite slabs heated by the near field result in large displacements and thermal expansion. The expansion of the composite slabs is subsequently restrained by the surrounding bays. As the fire

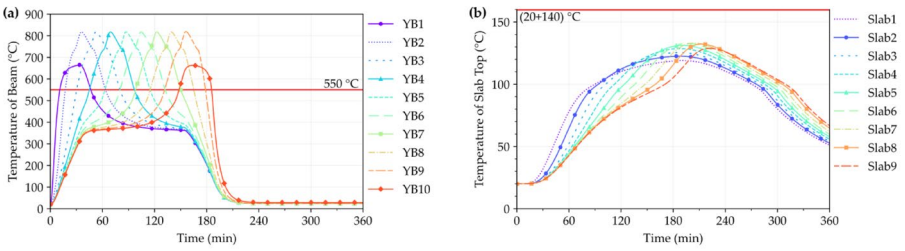

Fig. 13 Thermal response of the structural elements in 3D model under the travelling fire scenario 1 (fire spread rate: 2.5 mm/s): **a** YBeam1 to YBeam10; and **b** Slab1 to Slab9

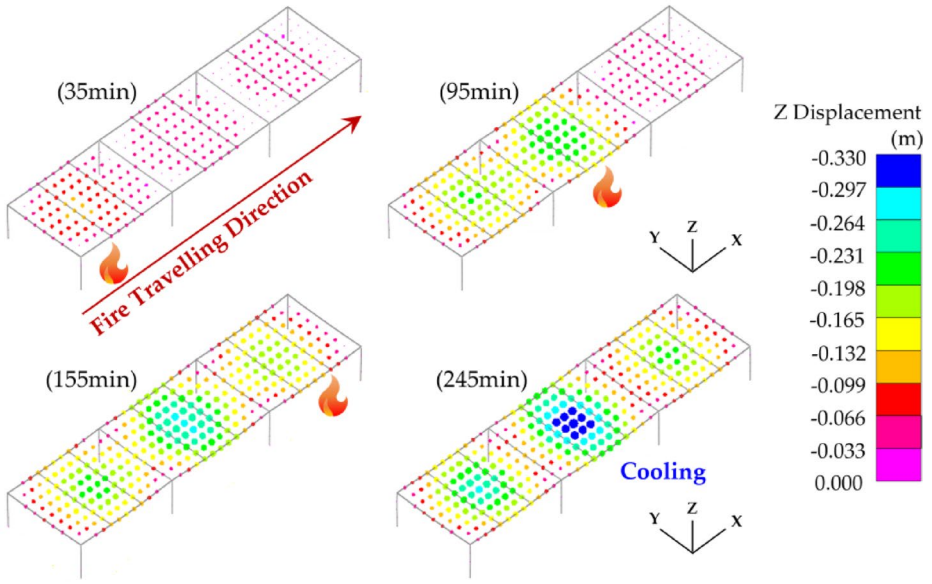

Fig. 14 Displacement contour of 3D model under the travelling fire scenario 1 (fire spread rate: 2.5 mm/s, fuel load density: 511 MJ/m^2, HRRPUA: 250 kW/m^2, and IOF: 9.6)

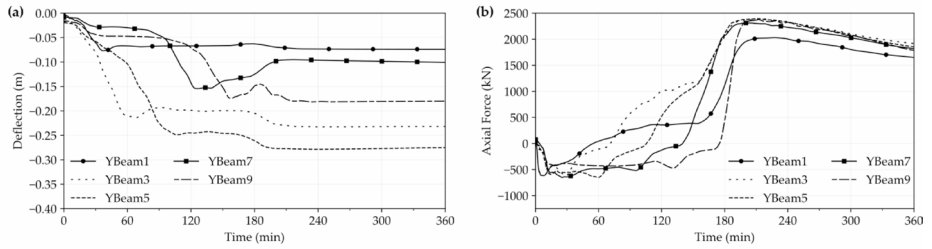

Fig. 15 Structural response of the YBeams (Y direction) in 3D model at mid-span under the travelling fire scenario 1 (fire spread rate: 2.5 mm/s): **a** Deflection; and **b** Axial force

is travelling away, the temperature continues penetrating the slab in-depth, hence yielding an even higher compression during the "local" cooling phase, see Fig. 16d. If the deflection is (artificially) increased by enhancing the mechanical loading to a higher magnitude, the composite slab is likely to present an apparent tensile membrane action, which features having a compressive ring supporting a central tensile region [53]. The observed irregularity in Figs. 16 and 20 is likely due to the presence of numerous blue and red vector icons, resulting in visual distortion.

3.2.2 Travelling Fire Scenario 2 (0.5 mm/s)

Travelling fire scenario 2 represents a design travelling fire scenario with a "slow" spread rate of 0.5 mm/s, yielding a modest total HRR of 1.5 MW.

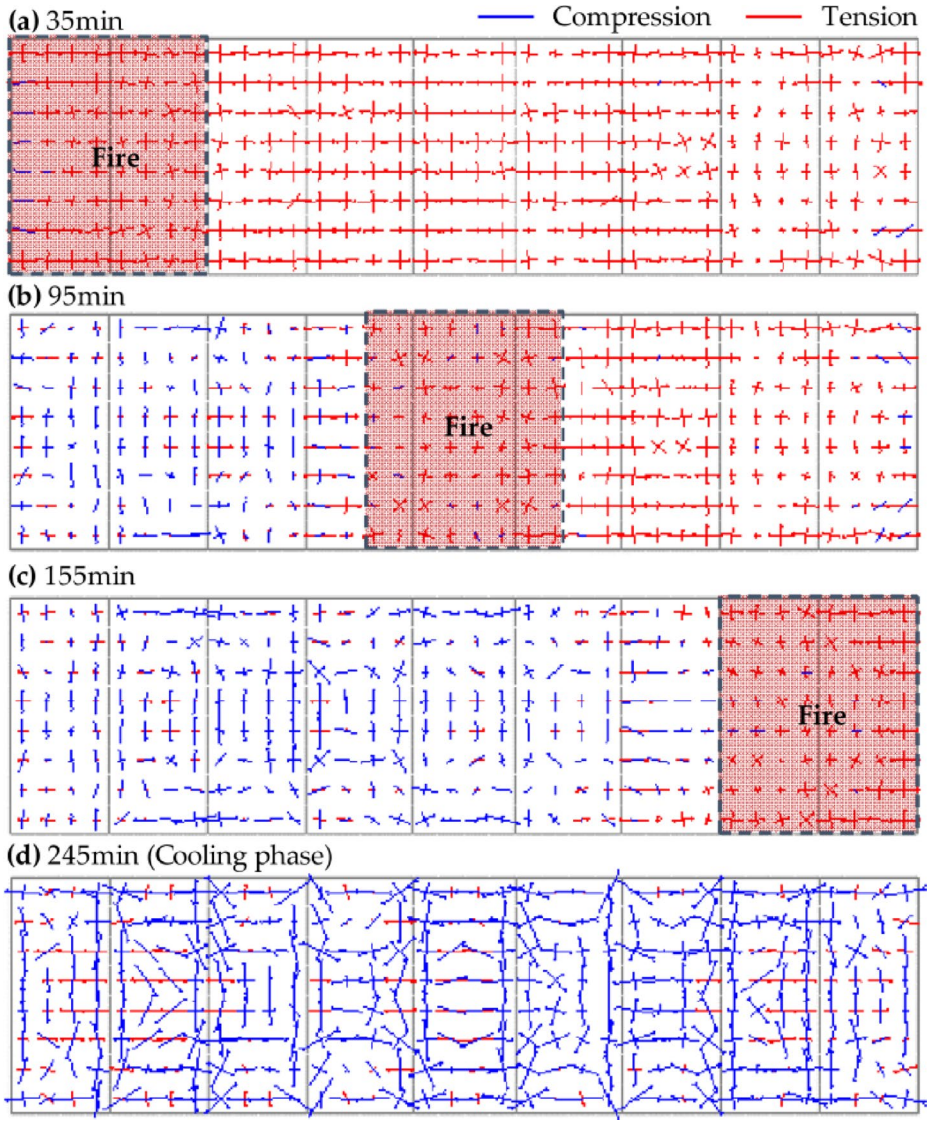

Fig. 16 Membrane tractions in the slab under the travelling fire scenario 1 (fire spread rate: 2.5 mm/s): **a** 35 min; **b** 95 min; **c** 155 min; and **d** 245 min

As shown in Fig. 17, under scenario 2, the peak lower flange temperature of the YBeams reaches 670 °C, exceeding the critical temperature of 550 °C. Further, the "distinguishable" full heating and cooling cycles are observed for all the structural elements. When the slow travelling fire approaches a structural member even with a modest total HRR, 1.5 MW, the longer near-field exposure (due to slow fire spread rate) would enable the fire more time to "heat up" the structural member, which may still result in more energy being absorbed by the structural member.

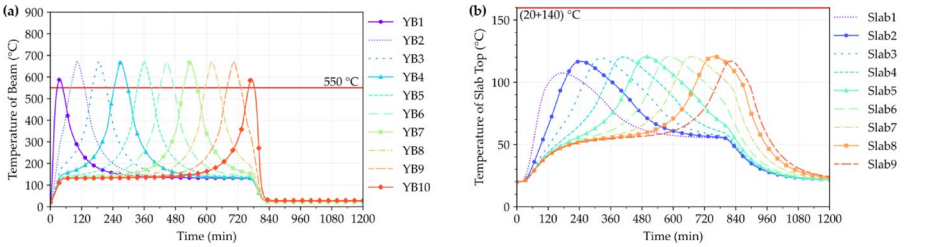

Fig. 17 Thermal response of the structural elements in 3D model under the travelling fire scenario 2 (fire spread rate: 0.5 mm/s): **a** YBeam1 to YBeam10 (Y direction); and **b** Slab1 to Slab9

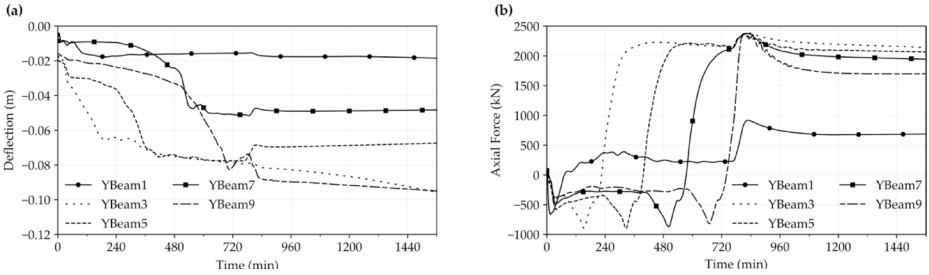

Fig. 18 Structural response of the YBeams (Y direction) in 3D model at mid-span under the travelling fire scenario 2 (fire spread rate: 0.5 mm/s): **a** Deflection; and **b** Axial force

Figure 18a presents the development of the YBeams deflection at mid-span under the scenario 2 (0.5 mm/s). The observed pattern is similar to the scenario 1 (2.5 mm/s), but the deflections are relatively smaller. For instance, under scenario 2, YBeam3 has the largest deflection, peaking at 0.097 m during the cooling phase. In comparison, YBeam5 experiences the largest deflection at 0.28 m under scenario (1) This difference is due to lower resultant HRR in scenario (2) This 1.5 MW fire impacts only a limited area of the structure, allowing the remaining structural members to maintain a relatively lower temperature, higher stiffness, and more effective load path redistribution.

The “axial force reversal” phenomenon is also observed under scenario 2, as shown in Fig. 18b. Notably, scenario 2 induces larger axial forces compared to those in scenario 1. For instance, YBeam7 undergoes significant axial forces, reaching 873 kN in compression and 2379 kN in tension at 502 min and 824 min, respectively. In contrast, under scenario 1, the same beam experiences 650 kN in compression and 2311 kN in tension at 25 min and 200 min, respectively. This difference is also attributable to the relatively modest 1.5 MW fire in scenario 2, which impacts a limited area of the structure, allowing adjacent cooler structural components to provide stronger restraint to the heated area. Even though the deflection of steel beams under the travelling fire scenario with a “slow” spread rate of 0.5 mm/s is significantly less (barely reaching 0.1 m), the high axial force is recorded during the cooling phase, as high as 2379 kN in Ybeam7. The high axial force causing the high utilisation of structural members’ capacity, meanwhile, could lead to the connections' failure, as experimentally identified by Dai et al. [54]. Consequently, this suggests that even “slow” travelling fires, which may appear less severe in fire size, however still should be

considered in performance-based structural fire design due to the associated very large axial force development.

The membrane tractions in slab of the 3D model at the selected times, i.e., 140 min, 400 min, 660 min and 840 min (cooling phase), under scenario 2, are presented in Fig. 19. In contrast to the membrane tractions presented in Fig. 16 for the scenario 1, more slab area is demonstrated in tension and there is a lower magnitude of compression during the cooling phase. This is because the fire size of scenario 2 is significantly smaller, i.e., approximately 6.0 m^2 with a modest total HRR of 1.5 MW, compared with 30 m^2 which has a total HRR of 7.5 MW.

3.3 Summary of the Comparative Analysis

This subsection evaluates the structural fire performance under various design fires, including standard fire, parametric fires and travelling fires. As Fig. 20 illustrates, YBeam7 is used as a representative structural member for this comparative analysis. This beam is prone to experience less favourable conditions due to several factors. YBeam7 is a primary beam, which normally bears a higher load demand than secondary beams. Considering the coupling effect of thermal and structural responses, YBeam7 is exposed to hot layer pre-heating for a considerable duration. Consequently, when the near-field of the travelling fire is beneath the YBeam7, its upper flange peak temperature reaches 664 °C, even with a modest fire size of 1.5 MW.

As presented in Fig. 20a, a key discrepancy between the temperature profiles under the standard fire and the parametric fires (Long-cool and Short-hot (with IOF 9.6)) arises from the inclusion of a cooling phase in parametric fire models. Nevertheless, the lack of fire protection leads to a structural collapse during the heating phase, under the situation of the uniform gas-phase temperature distribution within the compartment. As demonstrated in Figs. 8, 11 and 12, significant deflection of the steel beams occurs, theoretically reaching the critical deflection of 0.3 m (equivalent to L/20 for the YBeam with a length, L, of 6 m in this case), and is followed by "run-away" deflections, indicating structural collapse. As a result, the structural responses under these scenarios are similar, as presented in Fig. 20b. The major difference lies in the failure time of YBeam7, which stands at 6 min, 13 min and 18 min for the parametric fire (Short-hot (with IOF 9.6)), the parametric fire (Long-cool) and the standard fire (ISO 834), respectively.

However, Fig. 20 highlights notable differences between the thermal and structural responses under the uniform design fire scenarios and the travelling fire scenarios. These differences primarily stem from the spatially and temporally non-uniform gas-phase temperature distribution observed in the travelling fires. A significant structural response to fire only occurs when the near-field of the travelling fire approaches, as shown in Fig. 20b and c. For instance, YBeam7 has its largest deflections, 0.15 m at 126 min and 0.05 m at 786 min, under the travelling fire scenario 1 (2.5 mm/s) and the travelling fire scenario 2 (0.5 mm/s), respectively. Even under the scenario 1, with a fire spread rate of 2.5 mm/s and a fire size of 7.7 MW, the maximum deflection of YBeam7 is 0.15 m, which is still lower than the critical deflection of 0.3 m (i.e., 6 m/20, one-twentieth of the beam length).

Note that despite the relatively minor deflections under the travelling fire scenarios, the heating-cooling cycles induced by the travelling fires result in "axial force reversal" and a large tensile force during the cooling phase, which might cause unforeseen failure. For

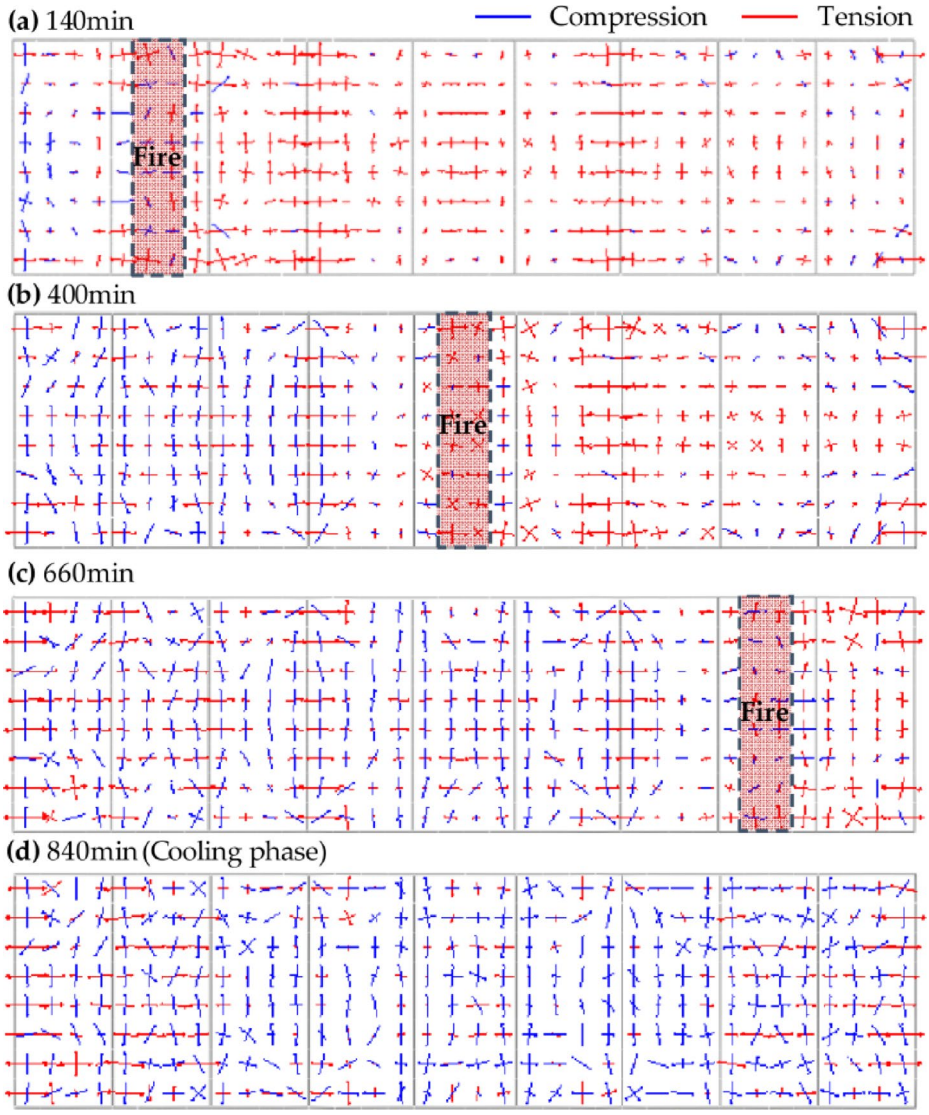

Fig. 19 Membrane tractions in the slab under the travelling fire scenario 2 (fire spread rate: 0.5 mm/s): **a** 140 min; **b** 400 min; **c** 660 min; and **d** 840 min

example, Fig. 20c shows that YBeam 7 undergoes maximum axial compression forces of approximately 600 kN during the heating phase of the uniform fire scenarios. Following the failure of beams and the subsequent structural collapse, the restraints are released, resulting in the axial forces approaching nearly zero. However, under travelling fire scenarios, YBeam7 experiences its highest axial compression forces, recorded at 650 kN and 873 kN. These peaks occur as the fire moves closer to, and directly beneath, YBeam7 at 25 min for scenario 1, and at 502 min for scenario 2, respectively. Furthermore, YBeam7 experiences "axial force reversal" during the cooling phase of the travelling fire scenarios. Specifically,

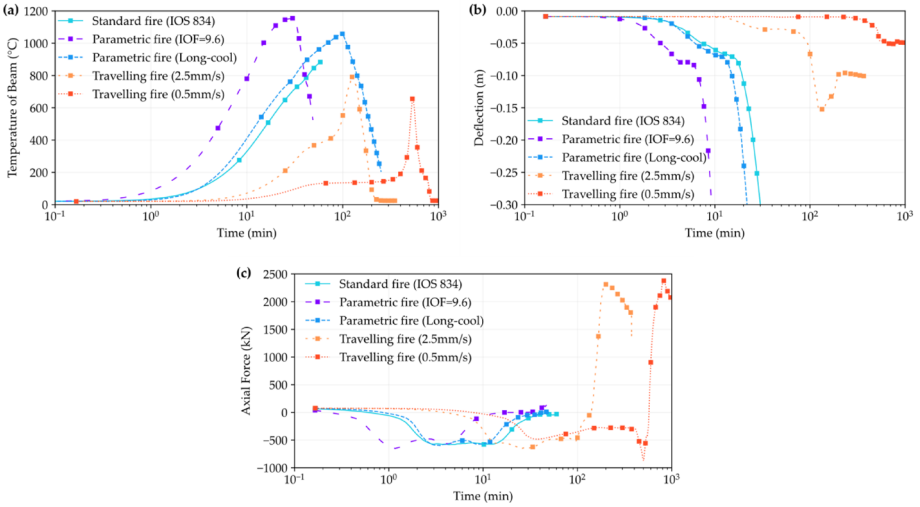

Fig. 20 Thermal and structural response of YBeam7 (Y direction) in 3D model at mid-span under various design fire scenarios: **a** Upper flange temperature; **b** Deflection; and **c** Axial force

during the cooling phase, the axial forces in YBeam7 escalates to a higher order of magnitude, reaching 2311 kN and 2379 kN in tension, for scenarios 1 and 2, respectively. This reversal is attributed to the contraction of the heated, expanded steel beams, which remains constrained by surrounding structural components. This observation underscores a significant difference between the uniform fire scenarios and the travelling fire scenarios in terms of structural fire responses. Given that uniform design fire scenarios may only encompass a limited variety of complex fire situations, incorporating travelling fire scenarios into performance-based structural fire design offers a more realistic approach to analysing structural fire responses.

4 The Significance of Slab

This study aims to improve numerical modelling for structural fire analysis by bridging the gap between simplified 2D models and more detailed 3D simulations. A key distinction is that the 3D structural model in this paper accounts for stiffness contributions from slabs, which are typically neglected in 2D models. While boundary conditions in full-scale structures remain a challenge, our focus is on understanding the fundamental differences between 2D and 3D approaches.

In this section, to maximise the structural deformation under different travelling fire scenarios for the 3D model against 2D models (i.e., 2D model with effective slab width and 2D steel frame model), all the structural steel members were still left unprotected. The effect of fire protection is further investigated in Sect. 5.

4.1 3D Model vs. 2D Models Under Travelling Fire Scenario 1 (2.5 mm/s)

Figure 21 presents the displacement contour development of the 2D models under the travelling fire scenario 1. Critical structural response events at specific time are selected and demonstrated: 35 min, 95 min, 155 min and 245 min for the 2D model with effective slab width (consistent with the 3D model), and 35 min and 75 min for the 2D steel frame model, respectively.

A comparison of Figs. 14 and 21 highlights that the global structural response and the potential structural failure mechanism could be fundamentally different between the 3D model and the 2D model. Specifically, under the scenario 1 (2.5 mm/s), as the fire moves through each bay, it induces the maximum deflection which subsequently decreases due to cooling once the fire has moved away. However, the maximum deflection in each bay of the 2D model with effective slab width is larger than 0.7 m, exceeding both the largest deflection of 0.33 m observed in the 3D model, and the critical deflection of 0.4 m, i.e., L/20, where L is the longest XBeam with length of 8 m. Interestingly, during the cooling phase, the deflections of Bay1 and Bay3, at 0.99 m and 0.95 m respectively, are larger than the 0.77 m recorded in Bay2. This is different with the 3D model, which exhibits the largest deflection in Bay2 during the cooling phase. The 2D model with effective slab width, reacting as a continuous three-span composite beam, allowed the middle span (Bay2) to be in favourable conditions, with lower bending moments. This reveals that the simplified 2D model, even when considering the slab with effective width, still deviates from the 3D structural response under travelling fires.

The structural collapse of the 2D steel frame model occurs at around 77 min under the scenario 1, see Fig. 21b. The maximum deflection of the XBeams reaches 1.31 m before its failure. This value is significantly larger than the critical deflection 0.4 m. In contrast, the largest deflection of the slabs of the 3D model reaches 0.33 m at the second bay during the cooling phase, with no indication of structural collapse (refer to Fig. 14). This is because the 3D model has higher overall stiffness due to the presence of the composite slab compared with the simplified 2D model.

Figure 22 shows the comparison of structural response between the 3D model and the 2D models under the travelling fire scenario 1. In Fig. 22, the largest deflection of XBeam1 and XBeam2 in the 2D steel frame model reaches 1.31 m and 0.96 m respectively (both far

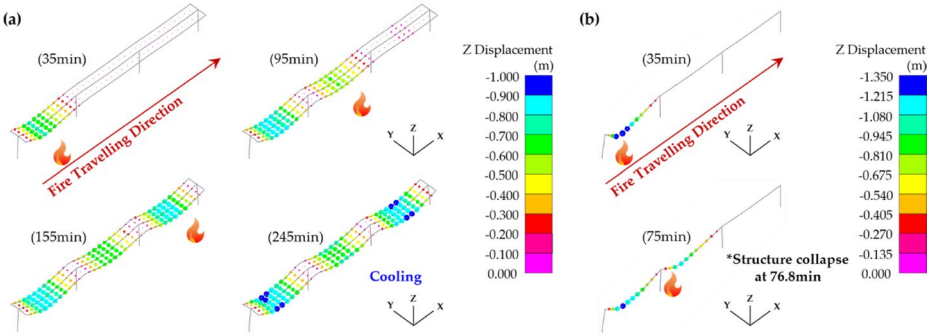

Fig. 21 Displacement contour under the travelling fire scenario 1 (fire spread rate: 2.5 mm/s, fuel load density: 511 MJ/m^2, HRRPUA: 250 kW/m^2, and IOF: 9.6): **a** 2D model with effective slab width; and **b** 2D steel frame model

beyond the critical deflection of 0.4 m), prior to the global structural collapse. In the 2D model with effective slab width, the largest deflection of the XBeams ranges from 0.67 m to 0.85 m, all higher than the critical deflection of 0.4 m. In contrast, XBeam2 in the 3D model has the largest deflection of 0.22 m, which was below the critical deflection.

Figure 23 presents the deflection rate at mid-span of the XBeams for the 3D model, the 2D model with effective slab width and the 2D steel frame model. Again, the comparisons of the three figures indicate a fundamental difference in the global structural responses between the 3D model and the 2D models. In the 3D model, the largest deflection rate of XBeam1 reaches 6.4 mm/min, significantly lower than the critical deflection rate, i.e., $L^2/9000d$, where L is the longest XBeam length of 8 m and d is the cross-sectional depth of 0.403 m. Whereas the largest deflection rates of the XBeams in the 2D model with effective slab width are all beyond the critical deflection rate of 18 mm/min. Furthermore, the largest deflection rates of XBeam1 and XBeam2 in the 2D model are over an order of magnitude higher. Note that the temperatures of most steel structural members exceed 600 °C, and up to 800 °C, under the travelling fire scenario 1. It means the loss of steel strength can be as high as 80–95% according to the Eurocode [32].

Figure 24 summarises the axial force and stress utilisation of the XBeams under travelling fire scenario 1 for 2D models against the 3D model. In Fig. 24b, the stress utilisation of the XBeams in the 2D model with effective slab width, and the 3D model, all approach to 1.0 during the cooling phase. The axial forces of XBeam1 to XBeam3 in the 3D model are 2180 kN, 2350 kN, and 2105 kN, respectively, close to the axial force capacity of N_{Rd} = 2448 kN (see Fig. 24a). In the 2D model with effective slab width, the axial forces of the XBeams peak within a range of 1118 kN and 1434 kN, which is roughly 40% less than the maximum axial force noted in the 3D model. In contrast, due to lack of neighbouring restraints and stiffness (from the slab and adjacent structural members), the 2D steel frame model collapses in a very early stage of the whole travelling fire duration, and the beam axial forces are also significantly lower compared with the values in the 3D model. These observations suggest that the inclusion of an effective slab width in the 2D model might provide a better representation.

In summary, the global structural response and potential failure mechanisms differ fundamentally between 3D and 2D models, both under traditional fire boundary conditions

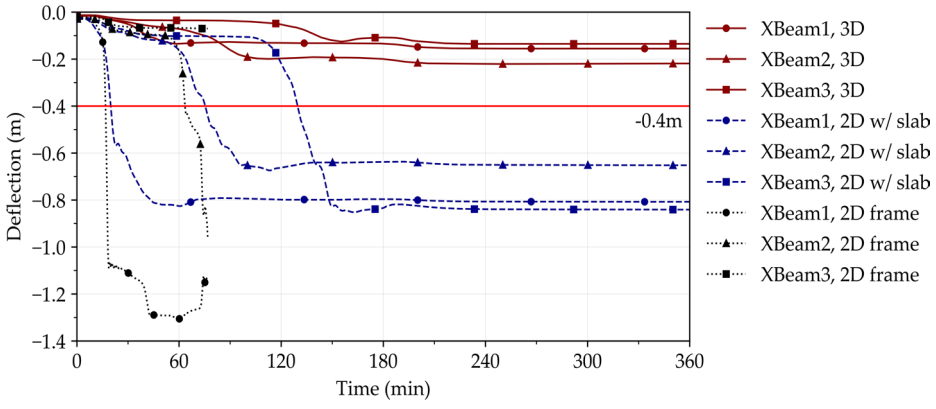

Fig. 22 Deflection of XBeam1 to XBeam3 (X direction) at mid-span under the travelling fire scenario 1 (fire spread rate: 2.5 mm/s), 3D model vs. 2D model with effective slab width vs. 2D steel frame model

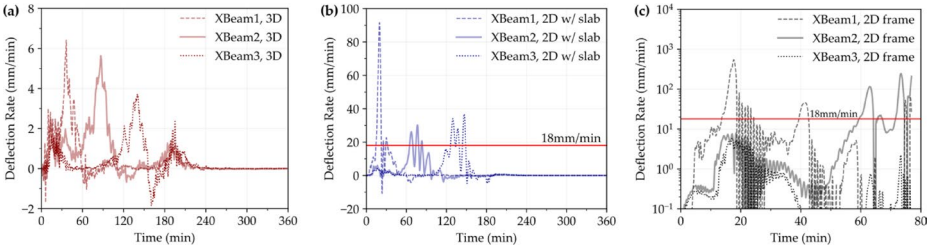

Fig. 23 Deflection rate of XBeam1 to XBeam3 (X direction) at mid-span under the travelling fire scenario 1 (fire spread rate: 2.5 mm/s): **a** 3D model; **b** 2D model with effective slab width; and **c** 2D steel frame model

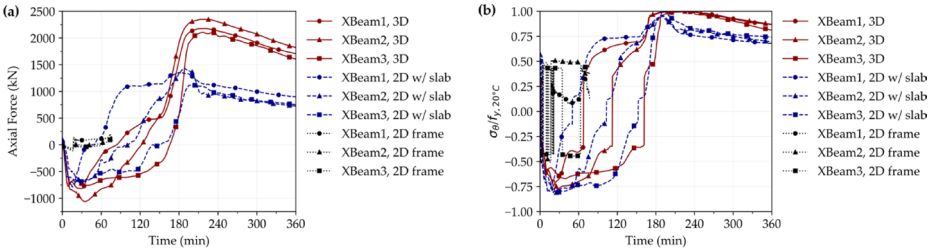

Fig. 24 XBeam1 to XBeam3 (X direction) at mid-span under the travelling fire scenario 1 (spread rate: 2.5 mm/s), 3D model vs. 2D model with effective slab width vs. 2D steel frame model: **a** Axial force; and **b** Stress utilisation: ratio of the axial stress envelope over the yield strength 355 MPa at 20 °C

(uniform or localised heating) [23, 24] and travelling fire scenarios [28]. Compared to the 3D model, 2D models tend to produce more conservative results, underestimating structural collapse resistance due to the absence of neighbouring restraints and stiffness from slabs and adjacent structural members. Although incorporating effective slab width in the 2D model provides a better representation of global structural responses and helps prevent early-stage collapse, the simplified 2D model (even with the effective slab width) still diverges from the 3D structural response under travelling fires. Notably, axial forces in the 2D model with effective slab width are approximately 40% lower than those in the 3D model. Additionally, the largest deflections during the cooling phase are only observed in the 3D model, as the 2D model with the effective slab width, functioning as a continuous three-span composite beam, places the middle span (Bay 2) into more favourable conditions with reduced bending moments.

4.2 3D Model vs. 2D Models Under Travelling Fire Scenario 2 (0.5 mm/s)

In Fig. 25, the maximal deflections for the XBeams are 0.07 m for the 3D model, 0.48 m for the 2D model with effective slab width, and 0.53 m for the 2D steel frame model. Compared with the structural response from scenario 1, lower deflections from travelling fire scenario 2 are observed, due to its slower travelling fire spread rate, 0.5 mm/s, and smaller fire size of 1.5 MW which could only "heat up" a limited number of structural elements. Note that the fire area is approximately 6 m^2 for this travelling fire scenario. This fire could only impact a limited area of the structure while the remainder of the structural bays remain at a relatively

lower temperature (pre-heated by the smoke temperature for the far field). Hence, the surrounding bays could still provide high stiffness and load redistribution paths to prevent the heated part of the structure from significant deflection.

As shown in Fig. 25, the largest deflections of the XBeams in the 3D model are between 0.06 m and 0.07 m. However, in the 2D model with effective slab width and the 2D steel frame model, these deflections are notably higher, ranging from 0.42 m to 0.48 m and from 0.47 m to 0.53 m, respectively. This marks difference in predicted deflections underlines the fundamental load-carrying role of the slab at elevated temperatures [38–40]. Specifically, in real structures composed of frames with primary beams and attached secondary beams, the slab forms an integral part of the load-bearing framework.

In addition, it is worth noting that there are "small plateaus" of deflection for the XBeams in the simplified 2D models, see Fig. 25. Such plateaus are attributed to the over-simplification of the 2D models, where the thermal expansion of the steel members (i.e., beams and columns) has an "interplay" effect on the overall deflection at the mid-span of the beams: the heated beams tend to deflect whereas the heated columns tend to lift-up the structural steel beams on top. For example, Fig. 26 demonstrates such an "interplay" effect in the 2D steel frame model, via decoupling the deflections for the beams and the vertical displacements of the heads of the columns, respectively. This effect is likely to be avoided in the 3D model due to the presence of the slab.

Further, lower deflection rates of the XBeams are found in the 3D model, below 0.8 mm/min as shown in Fig. 27a. In Fig. 27b, the 2D model with effective slab width demonstrates a higher deflection rate for the XBeams, reaching a maximum of 13.6 mm/min. However, this rate does not exceed the critical deflection rate of 18 mm/min. On the other hand, the failure of the XBeams could be determined according to the critical deflection rate being exceeded in the 2D steel frame model, see Fig. 27c. For instance, the peak deflection rates of the XBeams are 66 mm/min at 58 min, 29 mm/min at 309 min and 21 mm/min at 576 min for XBeam1, XBeam2 and XBeam3, respectively.

Figure 28 presents the axial force and stress utilisation of the XBeams under the travelling fire scenario 2. The 2D frame model has maximum axial forces of -105 kN and 251 kN for compression and tension, respectively, decreases by over 80% compared with the 2D model with effective slab width and the 3D model. More conservative axial forces are

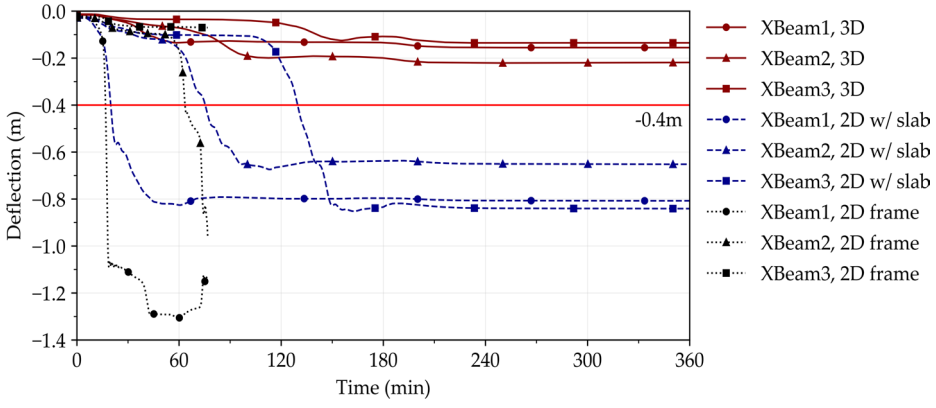

Fig. 25 Deflection of XBeam1 to XBeam3 (X direction) at mid-span under the travelling fire scenario 2 (fire spread rate: 0.5 mm/s), 3D model vs. 2D model with effective slab width vs. 2D steel frame model

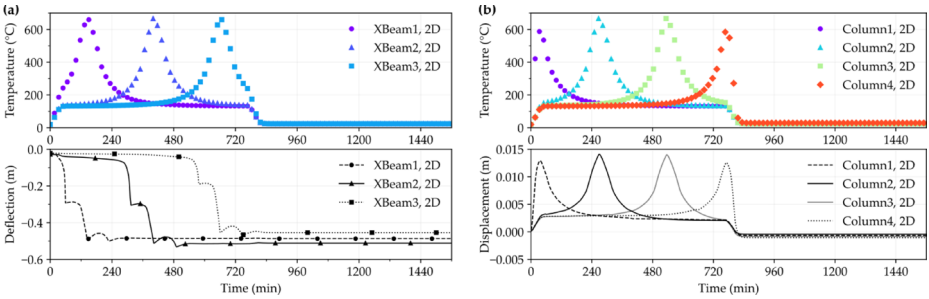

Fig. 26 Thermal and structural response of the steel beams in 2D steel frame model under the travelling fire scenario 2 (fire spread rate: 0.5 mm/s): **a** XBeam1 to XBeam3 (X direction); and **b** The vertical displacements of the heads of Column1 to Column 4

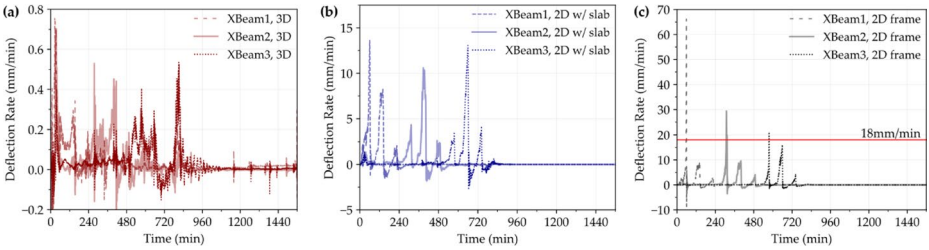

Fig. 27 Deflection rate of XBeam1 to XBeam3 (X direction) at mid-span under the travelling fire scenario 2 (fire spread rate: 0.5 mm/s): **a** 3D model; **b** 2D model with effective slab width; and **c** 2D steel frame model

captured by the models with slabs. This large force might result in the connections adopting a more unfavourable situation, i.e., the potential structural collapse triggered by the failure of the connections under such shear force [54], which is unlikely to be addressed in an over-simplified 2D steel frame model. Note that the "axial force reversal" and the increased tensile forces during the cooling phase are more apparent in the 2D model with effective slab width compared to the 3D model. This may arise from the absence of adjunctive primary beams and secondary beams in the 2D model with effective slab width. With these structural components in place, the 3D model allows for more reasonable load redistribution than the 2D model with effective slab width.

Furthermore, Fig. 28b shows that the stress utilisation of the XBeams in the 2D model with effective slab width and the 3D model are both above 70% and 90% in the heating phase and cooling phase, respectively. In contrast, only the stress utilisation of XBeam3 reaches 97% during the cooling phase in the 2D steel frame model. The results indicate that the simplification for modelling the composite structure as a 2D frame is not always the most conservative under travelling fires, in terms of internal forces. Further, compared with scenario 1 with a higher fire spread rate of 2.5 mm/s, the peak stress utilisation of the XBeams in the three models are all close to 1.0 under the travelling fire scenario 2.

In summary, under travelling fire scenario 2, characterised by a slower fire spread rate (0.5 mm/s) and a smaller fire size (1.5 MW), which heats only a limited number of structural elements, the differences in structural responses between the 3D and simplified 2D

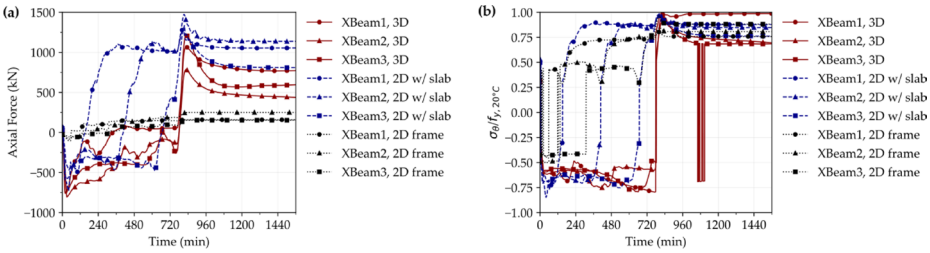

Fig. 28 XBeam1 to XBeam3 (X direction) at mid-span under the travelling fire scenario 2 (spread rate: 0.5 mm/s), 3D model vs. 2D model with effective slab width vs. 2D steel frame model: **a** Axial force; and **b** Stress utilisation: ratio of the axial stress envelope over the yield strength 355 MPa at 20 °C

models become more pronounced. This significant variation underscores the fundamental load-bearing role of slabs at elevated temperatures [22, 38–40]. The Cardington British Steel Corner Test demonstrated that the tensile membrane action of slabs plays a significant role at large deflections under extreme temperature [22]. During the heating phase, the concrete slab restrains the more rapidly heated steel beams, causing large, self-limiting deflections that lead to potential yielding of steel beams under axial compression. However, our numerical investigation of composite floors under travelling fires with "heating-cooling" cycles reveals that restrained deformations can affect structural behaviour in both heating and cooling phases. As shown in Figs. 24 and 28, "axial force reversal" occurs in steel beams during the "heating-cooling" cycles, with stress utilisation approaching 1.0 in the cooling phase, indicating a higher risk of beam failure under tension. This underscores the crucial load-bearing role of concrete slabs during both heating and cooling phases. For instance, the 3D model captures smaller deflections but exhibits more conservative axial forces, avoiding the "interplay" effect observed in the 2D steel frame model, caused by the coupling of beam deflections and vertical displacements at column heads. These findings suggest that simplifying composite structures into 2D models is not always the most conservative approach when considering the stress utilisation of steel members under travelling fires, particularly in scenarios involving "slow" travelling fires with limited heating areas. This implies that "slow" travelling fires are not advised to be ignored in performance-based structural fire design.

5 The Role of Fire Protection on 3D Model vs. 2D Models

This section investigates the effect of the performance-based fire protection design scheme on the structural response for both the 3D and 2D models under the travelling fire scenarios 1 and 2.

The mid-span thermal response of the YBeams is presented in Fig. 29, for scenario 1 (fire spread rate 2.5 mm/s) and scenario 2 (fire spread rate 0.5 mm/s), respectively. Note that the secondary beams are left unprotected. The peak temperatures of steel beams can be reduced effectively by fire protection. For instance, under the scenario 1, the peak temperature of YBeam7 decreases from 820 °C (without fire protection) to 540 °C (with fire protection); under the scenario 2, the peak temperature of YBeam7 with fire protection drops by 170 °C and the occurrence of the peak temperature is delayed by approximately 35 min.

Figure 30 a, c and e display the deflection for the 3D model, the 2D model with effective slab width and the 2D steel frame model, respectively, all under the travelling fire scenario 1. The figures contrast one case *without* any fire protection (w/o p) against the other case *with* fire protection (w/ p) for the primary beams and columns. It is found that the effect of fire protection on the deflection of the structure is significant, especially for the 2D steel frame model. As shown in Fig. 30a, upon the application of fire protection, the maximum deflection at the mid-span of the slabs in the 3D model decreases by around 50% on average. For instance, the maximum mid-span deflection decreases from 0.27 m (w/o p) to 0.13 m (w/ p), 0.33 m (w/o p) to 0.15 m (w/ p) and 0.21 m (w/o p) to 0.13 m (w/ p) for BAY1, BAY2 and BAY3, respectively. As depicted in Fig. 30c, the application of fire protection in the 2D model with effective slab width leads to an average reduction of approximately 80% in the maximum mid-span deflection of the XBeams. Furthermore, in the 2D steel frame model, Fig. 30e demonstrates that the fire protection prevents the collapse of the steel frame very effectively, such that the maximum deflection of XBeam2 at mid-span was only 0.15 m, which is far below the critical deflection of 0.4 m. It further proves that the fire protection of steel members plays a critical role to prevent the disproportionate collapse of the steel-framed structures when the slab is absent.

Figure 30 b, d and f present the deflection of the three structural models under the travelling fire scenario 2, for one case without any fire protection (w/o p) against the other case with fire protection (w/ p), for the primary beams and columns. In the 3D model, when the fire spread rate decreases to 0.5 mm/s in the travelling fire scenario 2, the effect of fire protection on the deflections becomes less significant, see Fig. 30b. The maximum deflection of slabs in the 3D model decreases by only approximately 11% on average. For instance, the maximum deflection at BAY2 decreases from 0.086 m (w/o p) to 0.074 m (w/ p). In contrast, Fig. 30d shows that the application of fire protection in the 2D model with effective slab width led to an average reduction of 68% in the maximum deflection of the XBeams. For example, the maximum deflection of XBeam2 is reduced from 0.42 m (w/o p) to 0.16 m (w/ p). Moreover, the maximum deflection of the XBeams decreases significantly once the fire protection is applied in the 2D steel frame model, i.e., from 0.501 m (w/o p) to 0.086 m (w/ p), 0.531 m (w/o p) to 0.119 m (w/ p) and 0.468 m (w/o p) to 0.087 m (w/ p), respectively, see Fig. 30f.

By comparing Fig. 30a and b, it can be seen that under scenario 1 with a higher spread rate of 2.5 mm/s, the largest deflection occurs in BAY2 with a longer span (i.e., 8.0 m). However, under the scenario 2 with a "slow" spread rate of 0.5 mm/s, the maximum deflections are likely to occur in the "side" bays of the 3D model (i.e., BAY1 and BAY3, as

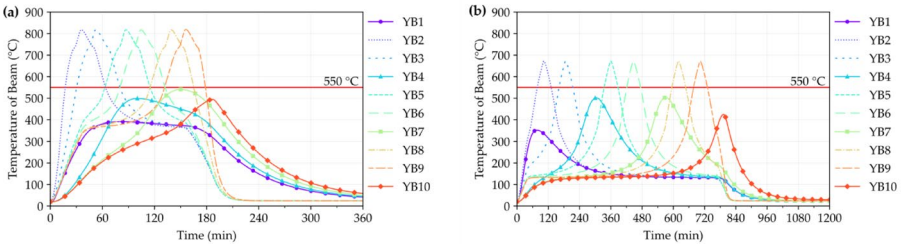

Fig. 29 Thermal responses of YBeam1 to YBeam10 (Y direction) in the 3D model under travelling fires, with fire protection of primary beams and columns: **a** scenario 1 (fire spread rate: 2.5 mm/s); **b** scenario 2 (fire spread rate: 0.5 mm/s)

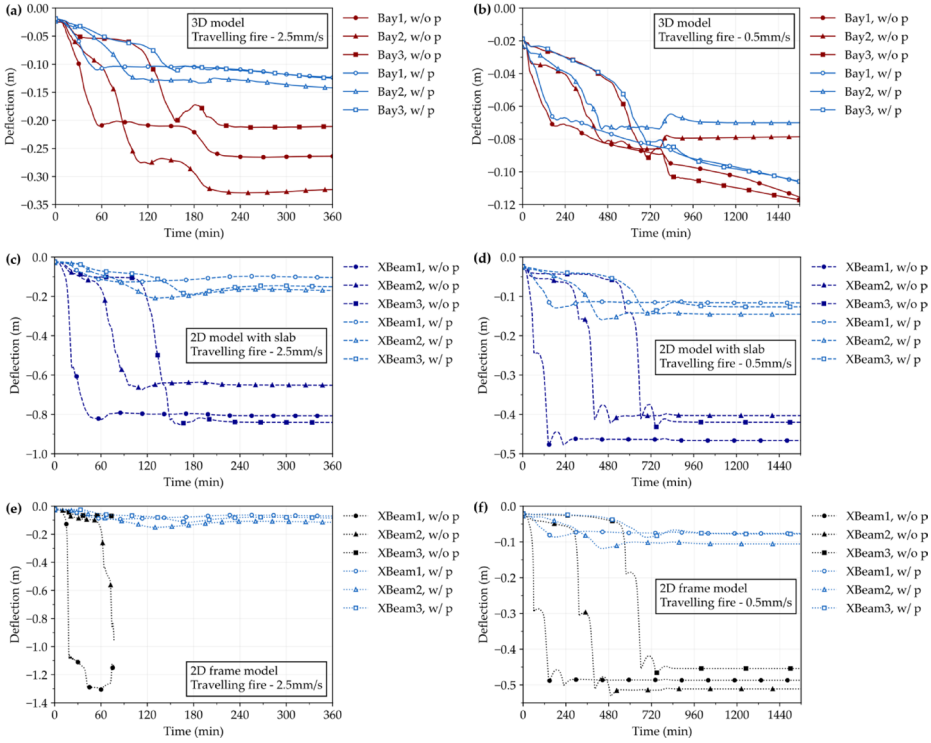

Fig. 30 Deflection under the travelling fire scenarios, without any fire protection (WOP) vs. with fire protection (WP): **a** 3D model under travelling fire scenario 1; **b** 3D model under travelling fire scenario 2; **c** 2D model with effective slab width under travelling fire scenario 1; **d** 2D model with effective slab width under travelling fire scenario 2; **d** 2D steel frame model under travelling fire scenario 1; and **f** 2D steel frame model under travelling fire scenario 2

described in Fig. 1a) instead of the longer bay (i.e., BAY2). This implies that the global structural response, or the potential structural failure mechanism, might be affected by the structural details (including with or without concrete slabs and the layout of the structure), in combination with the fire protection and the fire spread rate, simultaneously.

6 Conclusions

The application of finite element structural models to investigate the thermal and structural responses of large open-plan office compartments is demonstrated via an approach based on a representative "slice" of the structure, with a one-story prototype steel-framed structure with composite floors adapted based on the structural layout of the BST/FRS 1993 travelling fire test. The role of the slab must be considered, and insights into the impact on the FEM predicted structural responses under various design fires are obtained via investigating the difference among the 3D model, the 2D model with effective slab width and the 2D frame model. The sensitivity of fire conditions is assessed via study of the ISO834 standard fire, parametric fires (Long-cool and Short-hot (with IOF 9.6)), and two representative travelling

fire scenarios with spread rate of 2.5 mm/s and 0.5 mm/s, respectively. The performance is also sensitive to the effects of fire protection, assessed via a 3D model or simplified 2D models. The following specific findings are highlighted:

(1) The differences in structural responses under uniform design fires and travelling fires are highlighted by "axial force reversals" and the large tensile forces observed during the "heating-cooling" cycles of travelling fires. These effects result from the non-uniform temperature distribution in travelling fires, where the localised heating and expansion of steel beams, constrained by surrounding structural components, followed by cooling, cause the beams to be under tension. While cooling effects are also present in parametric fires, the unique impact of travelling fires is due to the movement of the fire, leading to sequential "heating-cooling" cycles. This underscores the importance of incorporating travelling fire scenarios into structural fire design for a more realistic, and more conservative, analysis of structural fire responses in large compartments.
(2) The global structural response, or the potential structural failure mechanism between the 3D model and the simplified 2D models, could be fundamentally different, and sometimes non-conservative, for the simpler 2D models. This result is likely to arise from differences in the layout of the structure, in combination with the fire protection and the fire spread rate, simultaneously.
(3) The 3D model is therefore critical for the performance-based structural fire design for travelling fires, via consideration of the importance of the slab, since simplified 2D models may not always provide the most conservative solution.
(4) Although the 2D models usually predict much larger deflections compared with the 3D model, they could significantly underestimate the large internal forces, which might potentially induce connections' failure in a more realistic scenario such as travelling fires.
(5) The "internal axial force reversal" caused by the heating-cooling cycles of travelling fires is more evident in the models with slabs, i.e., the 3D model and the 2D models with effective slab width.
(6) Due to the simplification of the 2D models omitting the significant stiffness contribution from the composite slab and the adjunctive structural components, the effect of the fire protection is likely to be amplified. Such a simplification may result in misleading results for performance-based structural fire design under different travelling fire scenarios.

Due to the above observations it is recommended that 3D models are always considered, as a minimum as a complement to simplified 2D models, to ensure robust structural fire analysis in scenarios involving travelling fires.

Acknowledgment This work is funded by Hong Kong Research Grants Council Theme-based Research Scheme (T22-505/19-N). The authors are also grateful to the fellowship supported by the Royal Academy of Engineering under the RAEng/Leverhulme Trust Research Fellowships programme (grant LTRF-2324-20-154) in the UK. For the purpose of Open Access, the author has applied a Creative Commons Attribution (CC-BY) licence to any Author Accepted Manuscript version arising. All data is provided in full in the results section of this paper.

Open Access This article is licensed under a Creative Commons Attribution 4.0 International License, which permits use, sharing, adaptation, distribution and reproduction in any medium or format, as long as

you give appropriate credit to the original author(s) and the source, provide a link to the Creative Commons licence, and indicate if changes were made. The images or other third party material in this article are included in the article's Creative Commons licence, unless indicated otherwise in a credit line to the material. If material is not included in the article's Creative Commons licence and your intended use is not permitted by statutory regulation or exceeds the permitted use, you will need to obtain permission directly from the copyright holder. To view a copy of this licence, visit http://creativecommons.org/licenses/by/4.0/.

References

1. Dai X, Welch S, Usmani A (2017) A critical review of travelling fire scenarios for performance-based structural engineering. Fire Saf J 91:568–578. https://doi.org/10.1016/j.firesaf.2017.04.001
2. Clifton GC (1996) Fire models for large firecells, HERA report R4-83. HERA, New Zealand
3. Stern-Gottfried J, Rein G (2012) Travelling fires for structural design-Part I: Literature review. Fire Saf J 54:74–85
4. Stern-Gottfried J, Rein G (2012) Travelling fires for structural design-Part II: Design methodology. Fire Saf J 54:96–112
5. Rackauskaite E, Hamel C, Law A, Rein G (2015) Improved formulation of travelling fires and application to concrete and steel structures. Structures 3:250–260. https://doi.org/10.1016/j.istruc.2015.06.001
6. Heidari M, Kotsovinos P, Rein G (2020) Flame extension and the near field under the ceiling for travelling fires inside large compartments. Fire Mater 44(3):423–436
7. Alpert RL (2016) Ceiling jet flows. In: SFPE Handbook of Fire Protection Engineering, Fifth Edition. Springer New York, pp 429–454
8. Rackauskaite E, Kotsovinos P, Jeffers A, Rein G (2017) Structural analysis of multi-storey steel frames exposed to travelling fires and traditional design fires. Eng Struct 150:271–287. https://doi.org/10.1016/j.engstruct.2017.06.055
9. Dai X, Welch S, Vassart O, Cábová K, Jiang L, Maclean J, Clifton GC, Usmani A (2020) An extended travelling fire method framework for performance-based structural design. Fire Mater 44:437–457. https://doi.org/10.1002/fam.2810
10. Hasemi Y, Yokobayashi Y, Wakamatsu T, Ptchelintsev A (1996) Modelling of heating mechanism and thermal response of structural components exposed to localised fires
11. Janssens ML (2000) Introduction to mathematical fire modeling. CRC
12. Horová K, Jána T, Wald F (2013) Temperature heterogeneity during travelling fire on experimental Building. Adv Eng Softw 62–63:119–130. https://doi.org/10.1016/j.advengsoft.2013.05.001
13. Charlier M, Franssen JM, Dumont F, Nadjai A, Vassart O (2021) Development of an analytical model to determine the heat fluxes to a structural element due to a travelling fire. Appl Sci (Switzerland) 11. https://doi.org/10.3390/app11199263
14. Alam N, Nadjai A, Charlier M, Vassart O, Welch S, Sjöström J, Dai X (2022) Large scale travelling fire tests with open ventilation conditions and their effect on the surrounding steel structure – The second fire test. J Constr Steel Res 188:107032. https://doi.org/10.1016/j.jcsr.2021.107032
15. Gamba A, Franssen JM (2021) GoZone: A numerical model for travelling fires based on cellular automata concept. Appl Sci (Switzerland) 11:10679. https://doi.org/10.3390/app112210679
16. Nan Z, Khan AA, Jiang L, Chen S, Usmani A (2022) Application of travelling behaviour models for thermal responses in large compartment fires. Fire Saf J 134:103702. https://doi.org/10.1016/j.firesaf.2022.103702
17. Dai X, Alam N, Liu C, Nadjai A, Rush D, Welch S (2024) Scaling-up fire spread on wood cribs to predict a large-scale travelling fire test using CFD. Adv Eng Softw 189:103589. https://doi.org/10.1016/j.advengsoft.2023.103589
18. Kotsovinos P, Rackauskaite E, Christensen E, Glew A, O'Loughlin E, Mitchell H, Amin R, Robert F, Heidari M, Barber D, Rein G, Schulz J (2023) Fire dynamics inside a large and open-plan compartment with exposed timber ceiling and columns: CodeRed #01. Fire Mater 47:542–568. https://doi.org/10.1002/fam.3049
19. Rackauskaite E, Kotsovinos P, Jeffers A, Rein G (2019) Computational analysis of thermal and structural failure criteria of a multi-storey steel frame exposed to fire. Eng Struct 180:524–543. https://doi.org/10.1016/j.engstruct.2018.11.026
20. Rezvani FH, Ronagh HR (2015) Structural response of a MRF exposed to travelling fire. Proc Inst Civil Eng Struct Build 168:619–635. https://doi.org/10.1680/jstbu.14.00046

21. Rackauskaite E, Kotsovinos P, Rein G (2017) Structural response of a steel-frame Building to horizontal and vertical travelling fires in multiple floors. Fire Saf J 91:542–552. https://doi.org/10.1016/j.firesaf.2017.04.018
22. Gillie M, Usmani AS, Rotter JM (2002) A structural analysis of the Cardington British steel corner test. J Constr Steel Res 58(4):427–442. https://doi.org/10.1016/S0143-974X(01)00066-9
23. Jiang J, Li GQ (2017) Disproportionate collapse of 3D steel-framed structures exposed to various compartment fires. J Constr Steel Res 138:594–607. https://doi.org/10.1016/j.jcsr.2017.08.007
24. Jiang J, Li GQ (2017) Progressive collapse analysis of 3D steel frames with concrete slabs exposed to localized fire. Eng Struct 149:21–34. https://doi.org/10.1016/j.engstruct.2016.07.041
25. Jiang J, Lu Y, Dai X, Li GQ, Chen W, Ye J (2021) Disproportionate collapse of steel-framed gravity buildings under travelling fires. Eng Struct 245:112799. https://doi.org/10.1016/j.engstruct.2021.112799
26. Kirby BR, Wainman D, Tomlinson LN, Kay T, Peacock BN (1999) Natural fires in large scale compartments. Int J Eng Performance-Based Fire Codes 1(2):43–45
27. ArcelorMittal (2024) Composite floor decking – Cofradal, product data sheet. https://construction-uk.arcelormittal.com/en/product/floors/composite-floors/cofradal (accessed 20/04/2024)
28. Nan Z, Dai X, Chen H, Welch S, Usmani A (2022) A numerical investigation of 3D structural behavior for steel-composite structures under various travelling fire scenarios. Eng Struct 267:114587. https://doi.org/10.14264/a1068ab
29. Horová K, Wald F (2015) Temperature heterogeneity of travelling fire and its influence on composite steel-concrete floor. Stavební Obzor - Civil Eng J 24(1). https://doi.org/10.14311/CEJ.2015.01.0006
30. Darwin D, Dolan CW, Nilson AH (2016) Design of concrete structures (Fifteenth). McGraw-Hill Education
31. CEN (2004) EN 1992-1-2:2004 - Eurocode 2. Design of concrete structures. General rules. Structural fire design. Brussels: European Committee for Standardization (CEN)
32. CEN (2005) EN 1993-1-2:2005 - Eurocode 3. Design of steel structures. General rules. Structural fire design. Brussels: European Committee for Standardization (CEN)
33. ARUP LSTC LS-DYNA features: reinforced concrete beams and shells with *MAT_CONCRETE_EC2. Livermore Software Technology Corporation
34. CEN (2008) EN 1994-1-2:2008 - Eurocode 4. Design of composite steel and concrete structures. General rules. Structural fire design. Brussels: European Committee for Standardization (CEN)
35. Tekla Structural Designer Composite beam effective width – online calculator. https://support.tekla.com/doc/tekla-structural-designer/2021/engh_composite_effective_width_calculations (accessed 20/04/2024)
36. Rackauskaite E, Kotsovinos P, Guillermo R (2017) Model parameter sensitivity and benchmarking of the explicit dynamic solver of LS-DYNA for structural analysis in case of fire. Fire Saf J 90:123–138. https://doi.org/10.1016/j.firesaf.2017.03.002
37. Orabi MA, Jiang L, Usmani A, Torero J (2022) The Collapse of World Trade Center 7: Revisited. Fire Technol 60(5):2963–2990. https://doi.org/10.1007/s10694-022-01225-2
38. Bailey CG (2001) Membrane action of unrestrained lightly reinforced concrete slabs at large displacements. Eng Struct 23:470–483. https://doi.org/10.1016/S0141-0296(00)00064-X
39. Usmani AS, Cameron NJK (2004) Limit capacity of laterally restrained reinforced concrete floor slabs in fire. Cem Concr Compos 26:127–140. https://doi.org/10.1016/S0958-9465(03)00090-8
40. Burgess I, Chan B (2020) An integrated yield-line approach to tensile and compressive membrane actions in thin lightly-reinforced concrete slabs. Eng Struct 208:110321. https://doi.org/10.1016/j.engstruct.2020.110321
41. Barrett BA (2013) Steel construction: fire protection. TATA Steel, British Constructional Steelwork Association (BCSA), UK
42. Franssen JM, Kodur V, Zaharia R (2009) Designing steel structures for fire safety. Taylor & Francis
43. CEN (2002) EN 1991-1-2:2002 - Eurocode 1. Actions on structures. General actions. Actions on structures exposed to fire. Brussels: European Committee for Standardization (CEN)
44. Choe L, Ramesh S, Dai X, Hoehler M, Bundy M, Bryant R et al (2021) NIST Technical Note 2165. Fire Research Division. Engineering Laboratory, National Institute of Standards and Technology, U.S. Department of Commerce. https://doi.org/10.6028/NIST.TN.2165. Fire Resilience of a Steel-Concrete Composite Floor System: Full-Scale Experimental Evaluation for U.S. Prescriptive Approach with a 2-Hour Fire-Resistance Rating (Test #1)
45. Lamont S, Usmani AS, Gillie M (2004) Behaviour of a small composite steel frame structure in a long-cool and a short-hot fire. Fire Saf J 39:327–357. https://doi.org/10.1016/j.firesaf.2004.01.002
46. Thomas PH, Heselden AJM (1972) Fully developed fires in single compartments. Fire Research Note No 923, Fire Research Station, Borehamwood, UK

47. Janssens ML, Birk DM (2000) An introduction to mathematical fire modeling, 2nd edn. Technomic Pub. Co., Lancaster, Pa.
48. ASTM, Standard test methods for fire tests of building construction and materials. ASTM E119 – 19, ASTM International, West Conshohocken, PA., (2019)
49. ASFP (2007) The Yellow Book - Fire protection for structural steel in buildings, 5th ed, Association for Specialist Fire Protection, UK
50. ASTM (2019) Standard specification for carbon structural steel. ASTM A36/A36M – 19. ASTM International, West Conshohocken, PA
51. Garlock ME, Quiel SE (2008) Plastic axial load and moment interaction curves for fire-exposed steel sections with thermal gradients. J Struc Eng 134:874–880. https://doi.org/10.1061/(asce)0733-9445(2008)134:6(874)
52. Morgan H (1979) Smoke control methods in enclosed shopping complexes of one or more storeys: a design summary. Building Research Establishment, Borehamwood, UK
53. Orabi MA, Qiu J, Jiang L, Usmani A (2022) Modelling concrete slabs subjected to localised fire action with opensees. J Struc Fire Eng 14(1):128–145. https://doi.org/10.1108/JSFE-05-2021-0033
54. Dai X, Choe L, Fischer E, Clifton GC (2024) Thermal and structural response of beam-end shear connections during a large compartment fire experiment. Fire Technol 60:3175–3207. https://doi.org/10.1007/s10694-023-01452-1

Publisher's Note Springer Nature remains neutral with regard to jurisdictional claims in published maps and institutional affiliations.

Authors and Affiliations

Zhuojun Nan[1] · Xu Dai[2] · Stephen Welch[3] · Asif Usmani[4]

✉ Xu Dai
xu.dai@liverpool.ac.uk

[1] Delft University of Technology, Delft, Netherlands

[2] University of Liverpool, Liverpool, UK

[3] University of Edinburgh, Edinburgh, UK

[4] Hong Kong Polytechnic University, Kowloon, Hong Kong